

Research paper

Application of Bayesian networks based on Sequential Monte Carlo simulation and physical model in fault diagnosis of horizontal three-phase separator system

Daqian Liu^a, Shangfei Song^{a,*}, Ting Huang^b, Siheng Shen^{a,c}, Xiaoping Li^a, Jing Gong^{a,**}

^a National Engineering Research Center of Oil and Gas Pipeline Transportation Safety / MOE Key Laboratory of Petroleum Engineering/Beijing Key Laboratory of Urban Oil and Gas Distribution Technology, China University of Petroleum-Beijing, Changping Beijing, 102249, China

^b Gas Hydrate and Marine Resources Strategic Research Center, CNOOC Research Institute Company Limited, Beijing, 100028, China

^c College of Information Science and Engineering/College of Artificial Intelligence, China University of Petroleum-Beijing, Changping District, Beijing, 102249, China

ARTICLE INFO

Keywords:

Bayesian networks
Fault diagnosis
Sequential Monte Carlo simulation
Horizontal three-phase separator
Physical model

ABSTRACT

In offshore production platforms, horizontal three-phase separator is common process equipment. Its main function is to complete the dehydration and degassing of crude oil. Separator system is more complex, and its failure may cause significant economic losses and disastrous consequences. Therefore, it is critical to accurately and quickly identify where and why faults occur in the separator system. In this study, separator fault diagnosis model based on Bayesian networks is developed. Moreover, Sequential Monte Carlo simulation and physical model are introduced to overcome field problems such as missing separator failure data and the inability of experts to provide accurate empirical knowledge. Using this model, 13 faults in a separator in an offshore crude oil processing system are successfully diagnosed. Meanwhile, the proposed model is compared with deep neural network, convolutional neural network, and deep residual network, with accuracy rates of 100%, 91.34%, 87.99%, and 94.62%, respectively. Then, the diagnostic accuracy of each model for different faults is also compared in this paper under various signal-to-noise ratios. The results show that the method proposed in this paper has better noise immunity compared to the other three models. Therefore, the accuracy and robustness of the proposed model is further demonstrated. Finally, to analyze the fault-tolerance of the proposed model, 2–3 error evidence is randomly entered. The results show that the proposed model has better fault tolerance compared to data-driven Bayesian networks.

1. Introduction

In recent years, continuous development of technology in the petroleum industry and increased offshore exploration activities have contributed to the increasing complexity of modern industrial systems (Dai and Gao, 2013; Gramling and Freudenburg, 2006). The horizontal three-phase separator system is one of the key sub-processes in the crude oil processing system and affects the product quality of the entire oil production system. In addition, there is a large amount of flammable and explosive liquid in the separator, and its failure could cause significant economic loss or even catastrophic consequences (Hou et al., 2020; Jiao et al., 2019). Therefore, timely completion of separator troubleshooting is essential for safe production of crude oil processing systems (Bartlett et al., 2009).

In general, fault diagnosis for process systems is mainly divided into physical model-based methods, signal processing-based methods and data-driven model-based methods (Shao et al., 2020). Their characteristics are mainly shown in Table 1. Physical model-based methods (Khaled et al., 2021; Li and O'Neill, 2018; Natarajan and Srinivasan, 2010; Zhang and Hong, 2017; Zhao et al., 2013a; An et al., 2011) rely largely on simulation or experimentation to model various faults to determine the type of fault in the system. However, physical model-based methods typically require a profound understanding of the process beforehand, followed by the simulating all types of faults in the system, which incur high costs for work. Moreover, physical model-based methods do not have a strong inference capability; it cannot rely on anomalous symptoms to reason the cause of faults. Signal processing-based methods (Guo et al., 2022; Wang et al., 2020; Feng

* Corresponding author.

** Corresponding author.

E-mail addresses: song.sf@cup.edu.cn (S. Song), ydgj@cup.edu.cn (J. Gong).

et al., 2017) aims to explore advanced signal denoising and filtering techniques to effectively highlight fault characteristics. However, signal processing based methods are susceptible to noise interference. Moreover, it cannot address all types of faults and has certain limitations in terms of applicability. Nowadays, data-driven models(Tang et al., 2024; Liu et al., 2024; Lou et al., 2022; Tan et al., 2021; Liu et al., 2023; Cheliotis et al., 2020; Li et al., 2022; Ren et al., 2016; Du et al., 2017; Indrawan et al., 2021; Kellil et al., 2023; Lin et al., 2023) are widely applied in the field of fault diagnosis and there have been notable achievements. However, data-driven models still have some drawbacks, such as high data dependency, poor interpretability, and poor adaptability. Although, many scholars(Ahmad et al., 2022; Hasan et al., 2021; Goodfellow et al., 2014; Metz et al., 2017; Chen et al., 2016; Odena et al., 2017; Figueroa Barraza et al., 2024; Grezmak et al., 2020; Liu, 2021; Yang et al., 2020) have made significant efforts to solve the above problems, however, many of the current results are only for specific scenarios and are not universal.

In recent years, Bayesian networks (BNs) have emerged as one of the leading algorithms for system fault diagnosis(Li et al., 2022). It is a probability-based modelling technique commonly used in expert knowledge-based fault diagnosis systems(Huang et al., 2008). It can integrate expert prior knowledge, historical data, and other incomplete and uncertain information. It is considered an ideal tool for knowledge representation, inference and prediction in dealing with uncertainty problems(Weber et al., 2012). In addition, BNs are good at solving the problems of missing data. This is because BNs can use other methods to finish parameter learning in the absence of available fault data. For example, expert experience(Cai et al., 2014; Huang et al., 2008; Zhao et al., 2013b) is used to determine the parameters of BNs; graph mapping is used to determine the parameters of BNs(Askarian et al., 2016; Gribaudo et al., 2015; Khakzad et al., 2011); the combination of many methods is used to determine the parameters of BNs(Cai, n.d.; Huang et al., 2020; Jing, 2022; Wang et al., 2022). More detailed statistics can be found in Table 2. In addition, BNs can be trained using discrete datasets. The construction of the simplest discrete datasets requires only expert experience and reasonable assumptions(Cai et al., 2016b). Meanwhile, BNs also have some advantages in terms of model interpretability. BNs use directed graphs to describe the causal relationships between variables. As a result, it can be very easy to explain causes of faults. For example, if node A points to node B, it can be intuitively considered that node A is the cause of the occurrence of node B. Therefore, BNs is chosen as the fault diagnosis model for the horizontal three-phase separator in this study.

However, two main challenges are faced in this study: 1) There is a lack of the separator failure data in the field to obtain the probability tables for the BNs. 2) Accurate expert knowledge cannot be provided by experts in the face of complex separator system. Therefore, to address these issues, Sequential Monte Carlo simulation (SMC) and physical model (PM) are introduced. SMC is an important numerical simulation method capable of dealing with uncertainty(Cheng et al., 2017) and adapted to non-linear and high-latitude problems(Liu et al., 2024). It

Table 1
Characteristics of the three diagnostic methods.

Method	Advantages	Disadvantages
Physical model-based methods	<ul style="list-style-type: none"> ● High accuracy ● High ● High interpretable ● High versatile ● High robustness 	<ul style="list-style-type: none"> ● Complex modelling ● The need for precise basic parameters ● High cost of work ● Weak reasoning skills ● Signal quality affected ● Inability to cover all possible fault types ● Dependent model assumptions
Signal processing-based methods	<ul style="list-style-type: none"> ● High real-time ● Wide diversity ● High automation 	<ul style="list-style-type: none"> ● High data dependency ● Weakly explanatory ● Weakly adaptable
Data-driven model-based methods	<ul style="list-style-type: none"> ● High adaptivity ● High real-time ● High accuracy 	

Table 2
The use of BNs in fault diagnosis.

Reference	Publication Year	Parameters Acquisition	Application
Huang et al.	2008	Expert experience	Vehicle
Khakzad et al.	2011	Fault tree mapping	Gas Process Facilities
Zhao et al.	2012	Expert experience	Water-cooled Centrifugal Chiller
Ferreiro et al.	2012	Expert experience Historical data	Aeroplane
Cai et al.	2013	Expert experience	Ground-source Heat Pump
Bouejla et al.	2014	Expert experience Historical data	Oil Field Installations
Cai et al.	2015	Expert experience	Subsea Pipe Ram BOP System
Gribaudo et al.	2015	Attack tree mapping	Railways
Cai et al.	2016	Expert experience	Subsea Production System
Askarian et al.	2016	Fault tree mapping Historical data	Chemical Plants
Cai et al.	2017	Markov state transfer relation	GMR Control Systems
Amin et al.	2018	Expert experience	Safety Critical Systems
Liu et al.	2019	Historical data	Subsea Blowout Preventer Control System
Vaddi et al.	2020	Expert experience	Nuclear Power Plant
Li et al.	2021	Data-driven	Building Energy System
Meng et al.	2022	Expert experience	Blowout Flow
Wang et al.	2022	Expert experience	Submarine Pipeline
Sahu and Palei	2022	Fuzzy theory	Dragline Subsystem
Xiao et al.	2023	Historical data	Unmanned Aerial Vehicles
Abdelhafidh et al.	2023	Expert experience	Industrial Water Pipeline
Kong et al.	2024	Expert experience	Subsea Blowout Preventer System

also has a highly efficient computing capability, which can significantly improve computing efficiency(Li et al., 2019; Migacz et al., 2019; O'Keeffe and Orkoulas, 2009). As a result of the above characteristics, SMC is often used for system state simulation in reliability analysis(Shan et al., 2023; Wangdee and Billinton, 2006; Wu and Li, 2019; Yu et al., 2018a, 2018b, 2021a, 2021b). At the same time, PMs are constructed based on rigorous mathematical formulas. Unlike human experts, it possesses high robustness and objectivity to avoid the influence of subjectivity on event assessment. In any field(Fernandez-de-Cossio-Diaz and Vazquez, 2018; Handel et al., 2020; Khaled et al., 2021; Talreja, 2016; Wu et al., 2022), it can replace human experts to provide fairly accurate and professional knowledge. Therefore, it is reasonable and feasible to use SMC and PM to solve the above problems: 1) SMC combines with PM can form discrete dataset for training BNs. 2) PM combined with fuzzy theory can replace human experts to provide the required parameters for BNs and reduce the cost of human experts. The overall structure of this paper is as follows:

- 1) **Section 2.** Introduce the separator process system, the physical model construction and the types of faults collected.
- 2) **Section 3.** Introduce the fault diagnosis method proposed in this paper.
- 3) **Section 4.** Perform fault diagnosis, model comparison and model fault-tolerance test.
- 4) **Section 5.** Summarize the paper.

2. Horizontal three-phase separator introduction

2.1. Process flow introduction

The main function of the horizontal three-phase separator is to realize dewatering and degassing of crude oil. Fig. 1 is a simplified flow diagram of a horizontal three-phase separator system. It consists mainly of an inlet valve, a separator, a gas-phase outlet valve, an oil-phase outlet valve, a water-phase outlet valve, a gas-phase proportional-integral-derivative (PID) actuator, an oil-phase PID actuator and a water-phase PID actuator. When the separator is working properly, it has a smooth inlet flow with no violent disturbances. To the left of the weir plate is Room I, which contains a mixture of oil, gas, and water. The water-phase is at the bottom, the oil-phase is in the middle, and the gas-phase is at the top. The right side of the weir plate is Room II and the internal main medium is oil. The water-phase level and the oil-phase level inside the separator will gradually reach the set value in a fault-free condition. Moreover, the PIDs for water-phase and oil-phase valves control the valve openings based on the water-phase level inside the separator and oil level in the Room II, the PID of the gas-phase valve controls the valve opening based on the pressure in the separator and ultimately ensuring the normal operation of the separator system. The separator's design basis parameters are shown in Table 3

2.2. Physical model construction

In this study, a physical model for a horizontal three-phase separator is established using the method proposed by Song et al. (2023). This physical model is developed using JAVA 8. The volumes of oil and water in Room I can be obtained from (1) and (2) respectively, and the level can be calculated from (3). The first part of (3) is the volume of the separator cylinder and the second part is the volume of the elliptical head at the edge of the separator.

$$V_l^{t+1} = V_w^t + V_o^t + (Q_{in,w}^t + Q_{in,o}^t - Q_{out,w}^t - Q_{out,o}^t) \times \Delta t \quad (1)$$

$$V_w^{t+1} = V_w^t + (Q_{in,w}^t - Q_{out,w}^t) \times \Delta t \quad (2)$$

$$V = L \left[\frac{D^2}{4} \arccos \left(1 - \frac{2H}{D} \right) - \sqrt{DH - H^2} \left(\frac{D}{2} - H \right) \right] + \frac{\pi h_i}{D} \left[\frac{D^2}{4} \left(H - \frac{D}{2} \right) - \frac{(H - D/2)^3}{3} + \frac{D^3}{12} \right] \quad (3)$$

Where, V is the volume of the liquid to left of the weir plate, m^3 . Q is the

Table 3
Horizontal three-phase separator design basis parameters.

Parameters	Maximum Design Value
Gas flow (Sm^3/h)	2860
Oil flow (m^3/h)	145
Water flow (m^3/h)	701
Operating pressure (kPaG)	1350
Operating temperature ($^\circ\text{C}$)	38–60
Design pressure (kPaG)	1900
Design temperature ($^\circ\text{C}$)	90

flow of liquid, m^3/s . Δt is the time step, s. L is the length of the left part of the weir plate in the separator, m. D is the diameter of the separator cylinder, m. H is the liquid level, m. h_i is the surface width of the elliptical head, m. Subscripts l , w and o indicate total liquid, water, and oil respectively. Subscripts t and $t+1$ indicate the current time step and the next time step, respectively. Subscripts in and out indicate input parameters and output parameters, respectively.

The separator pressure can be calculated from (4) and (5).

$$n^{t+1} = n^t + \frac{(Q_{in,g}^t - Q_{out,g}^t) \rho_g \Delta t}{M_g} \quad (4)$$

$$p^{t+1} = \frac{zRT^{t+1}n^{t+1}}{V_g^{t+1}} \quad (5)$$

Where, n is the molar amount of gas in the separator, mol. ρ_g is the gas density, kg/m^3 . M is the molar mass, kg/mol . P is the separator pressure, Pa. z is the compression factor calculated from the Peng-Robinson equation of state(Peng and Robinson, 1976). R is the gas constant, 8.314 $\text{J}/(\text{mol}\cdot\text{K})$. T is the temperature, K. Subscript g indicates gas.

The results of the comparison between the ASPEN HYSYS V12 (Khaled et al., 2021; Wu et al., 2022) physical model and the physical model used in this paper are shown in Fig. 2. From Fig. 2, data from both the physical model used in this paper and HYSYS are almost stable after 500s. Furthermore, the maximum relative error between the two is 5.5%, which is within the allowable engineering error of 10%(Hu et al., 2013; Sevee, 2010). Therefore, it can be believed that the physical model used in this paper is highly accurate and the working states it simulates are highly credible. The physical model used in this paper can provide strong support for subsequent research.

2.3. Fault and process parameters determination

By investigating the fault logs of the horizontal three-phase separator in subsection 2.1, 13 fault types are identified. They are Inlet Disturbance (ID), Water Valve Leakage (LEAK_w), Water Valve Blockage

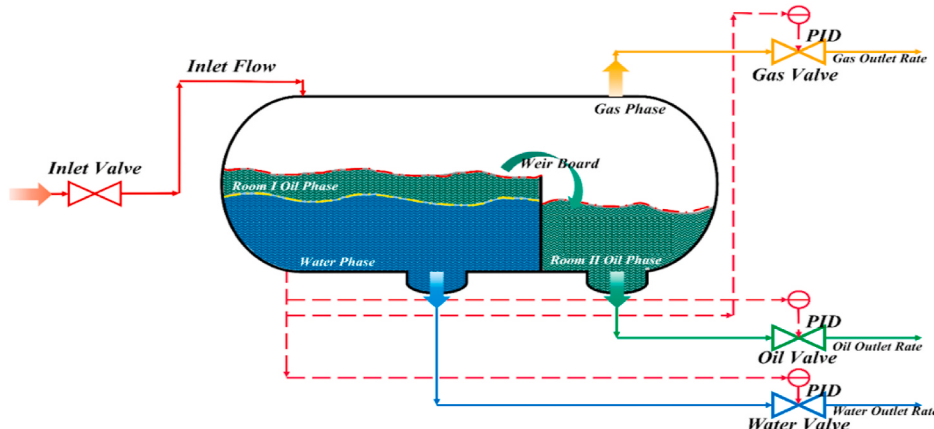


Fig. 1. Separator system process flow.

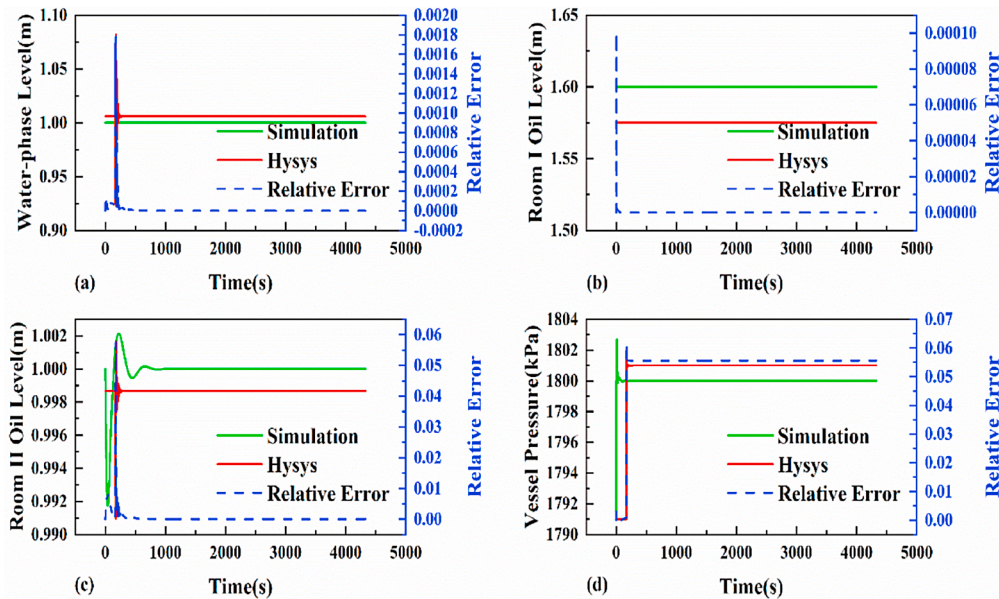


Fig. 2. Comparison results of the physical model used in this paper with HYSYS. (a) Water-phase level comparison results. (b) Room I oil level comparison results. (c) Room II oil level comparison results. (d) Vessel pressure comparison results.

($BLOCK_w$), Oil Valve Leakage ($LEAK_o$), Oil Valve Blockage ($BLOCK_o$), Gas Valve Leakage ($LEAK_g$), Gas Valve Blockage ($BLOCK_g$), Water Valve Actuator Fully Open (AFO_w), Water Valve Actuator Fully Closed (AFC_w), Oil Valve Actuator Fully Open (AFO_o), Oil Valve Actuator Fully Closed (AFC_o), Gas Valve Actuator Fully Open (AFO_g) and Gas Valve Actuator Fully Closed (AFC_g). Furthermore, the separator system is a small process system. If the system fails, its parameters will also change. For example, if the separator outlet oil-phase valve becomes blocked, the flow behind the oil valve will decrease and the oil level in Room II will gradually rise over time. Over time, Room II will gradually fill with the oil. It causes the oil-phase in Room II to pass through the weir plate, raising the level of the oil-phase in Room I. Also, as the valve blocks, the pressure in the separator and its inlet gradually increases and the inlet flow will decrease. The fault is simulated and analyzed using the physical model mentioned in subsection 2.2 and the results are shown in Fig. 3. Each parameter in the system has its own characteristics of change when different faults occur in the system. Therefore, 11 parameters are selected to describe the fault symptoms. They are Water Level (WL), Room I Oil Level (RIOL), Room II Oil Level (RIIOL), Vessel Pressure (VP), Water Valve Opening (WVO), Oil Valve Opening (OVO), Gas Valve Opening (GVO), Water Outflow Rate (WOR), Oil Outflow Rate (OOR), Gas Outflow Rate (GOR) and Inlet Flow (IF) respectively. And the variation characteristics of each parameter are classified into four states: Normal (N), High (H), Low (L), and Shock (S) (Liu et al., 2020).

3. Fault diagnosis methodology

3.1. Proposed fault diagnosis methodology

Based on the content of Section 2, a fault diagnosis method for horizontal three-phase separator is proposed, and the flow of the method is shown in Fig. 4: 1) The structure of fault diagnosis model is defined. The structure of a Bayesian network fault diagnostic model for a horizontal three-phase separator system is determined based on the cause of the fault, process parameters and states of parameters. 2) SMC and PM are used to generate dataset for training Bayesian networks. Failure rate data, repair rate data, and SMC are used to determine changes in system states. The simulation results of SMC are input into PM to obtain

simulation data. The simulation data is discretized to obtain a dataset for training Bayesian networks. This step is primarily used to solve the problem of missing field operating data. 3) PM and fuzzy theory are used to further provide the parameters required for Bayesian networks. PM is combined with fuzzy theory, which not only overcomes the shortcomings of SMC to further refinement of CPTs for Bayesian networks but also improves the modelling efficiency and fault tolerance of fault diagnosis model. 4) Diagnostic rules are developed, and fault diagnosis is completed. The fault diagnosis of the horizontal three-phase separator is achieved based on the posteriori probabilities provided by the fault diagnosis model and the fault diagnosis rules made by the field expert.

3.2. Fault diagnosis model structure determination

BNs are directed acyclic graphs, typically comprising nodes, directed edges, and conditional probability tables. A simple Bayesian network is illustrated in Fig. 5. Nodes represent system variables, directed edges denote dependencies or causal relationships between variables, and conditional probability tables describe relationships between each node and its parent nodes. Therefore, BNs have significant advantages in solving uncertain problems and explaining the causes of faults. This is one of the reasons why Bayesian networks is used in this study for fault diagnosis of horizontal three-phase separator.

In this study, two-layer BNs are designed for the separator system using NETICA(Cai et al., 2014; Xiao et al., 2023). The first layer is the fault layer and the second layer is the fault symptom layer(Cai et al., 2016b). The fault layer is mainly used to determine faults occurring in the system and consists of 13 faults. Each fault node has two states, Absent and Present. The fault symptom layer is mainly used to characterize faults and consists of 11 parameters. Therefore, the structure of the fault diagnosis model is shown in Fig. 6.

3.3. Fault diagnosis model parameters determination

Based on Subsection 3.2, this section focuses on the use of SMC and PM to determine the parameters of model.

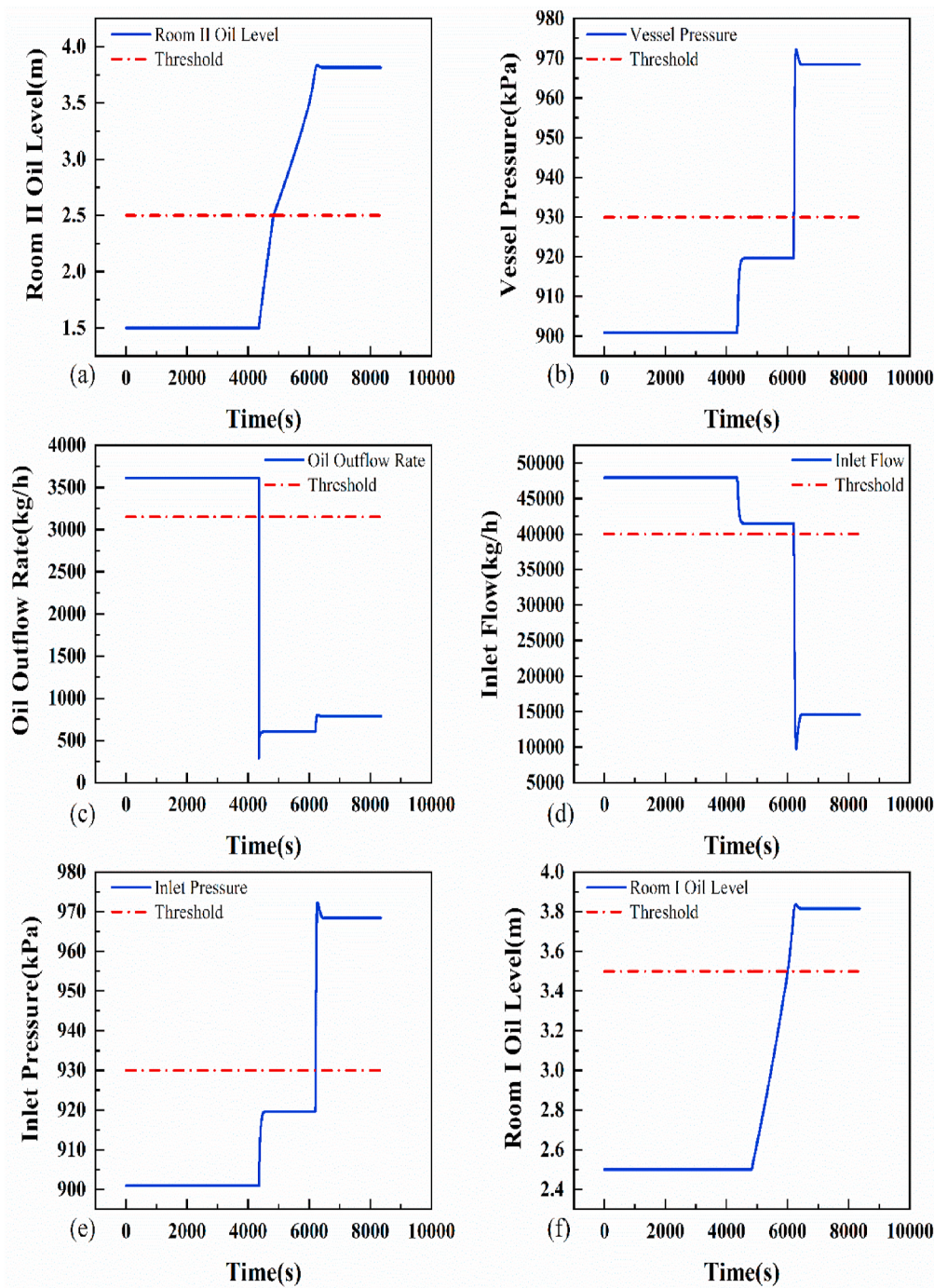


Fig. 3. Characteristics of the variation of six Parameters over time during oil valve blockage fault. (a) Room II Oil Level. (b) Vessel Pressure. (c) Oil Outflow Rate. (d) Inlet Flow. (e) Inlet Pressure. (f) Room I Oil Level.

3.3.1. Parameter determination based on SMC

3.3.1.1. SMC introduction. SMC is the most widely used data assimilation algorithm, which uses Bayesian inference and sampling techniques to recursively estimate system states. This means that by sampling durations, SMC can easily simulate time-dependent problems(Alves et al., 2020). Moreover, it is a non-parametric filter and can efficiently handle complex analogue models(Wu, 2017). Therefore, SMC can be used to simulate abnormal operating states in a system(Sankarakrishnan and Billinton, 1995). SMC are divided into Direct Monte Carlo Simulation (DMC) and Indirect Monte Carlo Simulation (IDMC) (Labeau and Zio, 2002). DMC relies on the unit's transition core distribution to determine

the state of the entire system. Therefore, DMC is more suitable for the case where the lifetime distribution of all units is known. IDMC relies on the transfer core distribution of the system to determine the state of the system. Therefore, IDMC is more suitable for cases where the system lifetime distribution is known(Zio, 2013). As the lifetime distribution of each unit in the separator system is different, it is more cumbersome to construct the transfer core of the system using IDMC. Instead, DMC is more appropriate for this situation. Therefore, DMC is chosen to simulate the state changes of the separator system in our study. DMC samples the transition times that may occur for all units in the system. Then, these transitions are sorted in ascending order on the timeline according to the time at which the transition occurs. The unit corresponding to the

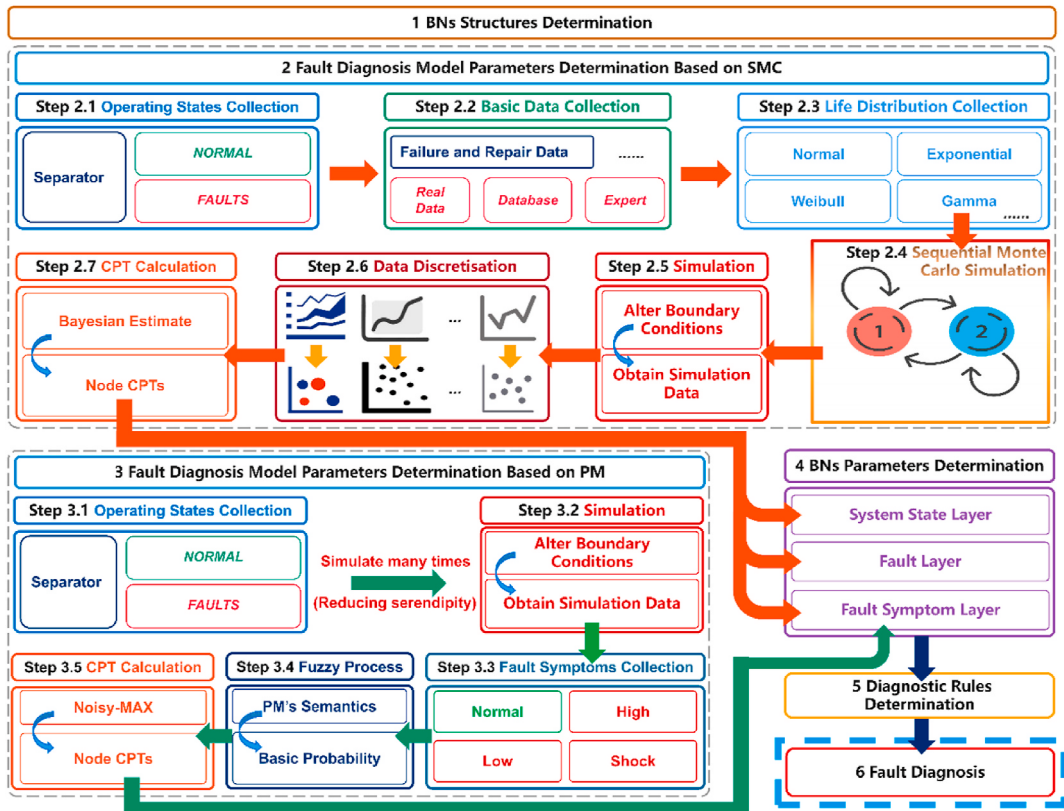


Fig. 4. Flow chart of the proposed fault diagnosis methodology.

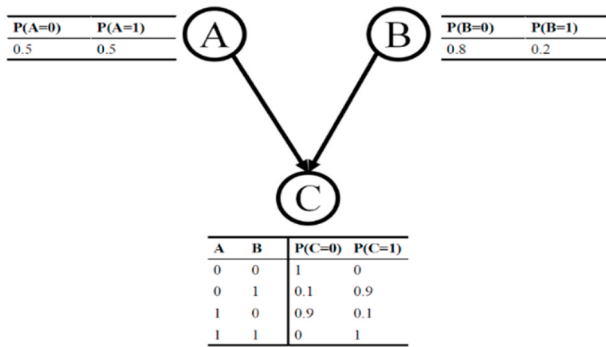


Fig. 5. Simple Bayesian networks.

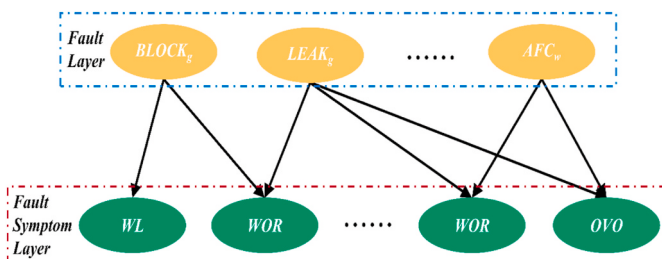


Fig. 6. Fault diagnosis model structure.

first transition on the timeline is the unit that actually undergoes the transition(Zio, 2013).

A simple case is used to further illustrate the DMC process. Suppose there are three units A, B and C in the system. And each unit has three states 1, 2 and 3, and each unit obeys an exponential distribution. When

the system is at $t = 0$, the states of three units are $A = 1, B = 1$ and $C = 1$. First, (6) is used to sample the occurrence time of all possible unit transitions:

$$t_{1 \rightarrow m_i}^i = t_0 - \frac{1}{\lambda_{1 \rightarrow m_i}^i} \ln(1 - R_{t,1 \rightarrow m_i}^i), \quad i = A, B, C \quad (6)$$

Where, t_0 represents the initial time of the system; $t_{1 \rightarrow m_i}^i$ represents the time when unit i is transferred from state 1 to state m_i ; $\lambda_{1 \rightarrow m_i}^i$ represents the transfer rate of unit i from state 1 to state m_i ; $R_{t,1 \rightarrow m_i}^i \sim U[0, 1]$.

Then, arrange these points in ascending order from $t_{min} \leq T_M$. Where, T_M is the simulation time of the system. Suppose t_{min} corresponds to failure state 2 of unit A, that is, $t_{min} = t_{1 \rightarrow 2}^A$. Then another transition time $t_{1 \rightarrow 3}^A$ sampled from unit A is deleted from the timeline. The current time shifts to $t_1 = t_{1 \rightarrow 2}^A$, and the states of three units in the system are $A = 2, B = 1$, and $C = 1$ respectively. The above is the process of performing a unit state extraction using DMC. Fig. 7 is a simplified schematic of the case.

3.3.1.2. SMC application. Based on Subsection 3.3.1.1, DMC and the principle of equivalent ignorance(Jeffreys, n.d.) are used in this study to simulate the variation of the separator system with time. Firstly, and most importantly, the distribution and associated parameters that each unit's life follows need to be determined. However, these parameters often face the problem of missing data. Therefore, this problem can be solved by making reasonable assumptions or by consulting the equipment manufacturer. These assumptions can be based on published papers(Cai et al., 2015), books(Calixto, 2016; System Reliability Theory), reliability databases(Gjerstad, 1985), etc. Also, the equipment manufacturer knows the equipment better than the field engineer. Therefore, a priori knowledge of the life of each unit can be determined by consulting the equipment manufacturer(Cai et al., 2014, 2015). In this study, separator parameters are provided by Zhou et al. (2022), actuator

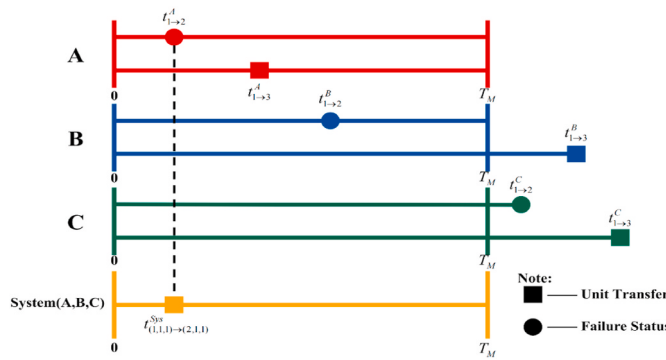


Fig. 7. Simple example of DMC.

parameters are provided by the on-site engineer and valve parameters are provided by Cai et al. (2015). These data are shown in Table 4. Then, this priori knowledge is used as input to the DMC to simulate changes in system state.

In this subsection, a case study is illustrated to better understand how system state transfer is determined by DMC: 1) The states of the units are determined. In this study, 0 indicates that the unit is in a normal state and 1 indicates that the unit is in an abnormal state. 2) The initial state of each unit is determined. A separator system mainly consists of a separator unit, oil, gas, and water valve units and three PID actuator units. At the initial moment, it is assumed all their states are normal, i.e., as shown in (7):

$$[U_1, U_2, U_3, U_4, U_5, U_6, U_7] = [0, 0, 0, 0, 0, 0, 0] \quad (7)$$

Where U_1 indicates the separator unit's state, U_2 indicates the oil valve unit's state, U_3 indicates the gas valve unit's state, U_4 indicates the water valve unit's state, U_5 indicates the oil valve's PID actuator unit's state, U_6 indicates the gas valve's PID actuator unit's state and U_7 indicates the water valve's PID actuator unit's state. 3) The transfer time for each unit is determined. Since all units are currently in a normal state, each unit can only change from 0 to 1 for a state transition. The separator unit and actuator units are Poisson distribution, the failure rate data and (6) can be used to determine their transfer time. Valve units are Weibull distribution, and their transfer time can be generated based on the scale and shape parameters. In this case, the calculation result of the transfer time for each unit is (8):

$$[T_1, T_2, T_3, T_4, T_5, T_6, T_7] = [21782, 5763, 50029, 27123, 5721, 6009, 7102] \quad (8)$$

Where, T_1 indicates the separator unit's transfer time, h. T_2 indicates the oil valve unit's transfer time, h. T_3 indicates the gas valve unit's transfer time, h. T_4 indicates the water valve unit's transfer time, h. T_5 indicates the oil valve's PID actuator unit's transfer time, h. T_6 indicates the gas valve's PID actuator unit's transfer time, h. T_7 indicates the water valve's PID actuator unit's transfer time, h. 4) The unit where the state transition occurred is determined. Based on subsection 3.3.1.1, the unit in which the state transition occurs has the shortest state transition time. Therefore, in this case, the unit in which the state transfer takes place is oil valve's PID actuator unit, i.e., a fault occurs in the oil valve's PID

Table 4
Unit lifetime distribution and parameters statistical results.

Unit	Distribution Type	Parameters
Separator	Poisson distribution	Failure rate: 0.0000132 Repair rate: 0.01389
Actuator	Poisson distribution	Failure rate: 0.0000175 Repair rate: 0.01042
Valve	Weibull distribution	Scale: 6800 Shape: 2.3

actuator in the separator system currently. 5) The specific type of fault is determined. Step 4 merely indicates that a fault has occurred in the oil valve's PID actuator, but the specific type of fault is not identified. Therefore, this problem is solved by introducing the principle of equivalent ignorance. In this study, a roulette wheel is designed that indicates the occurrence of AFO fault when the random number falls between 0 and 0.5 and the occurrence of AFC fault when the random number falls between 0.5 and 1. In this case, the random number is 0.1768, which is in the range 0–0.5, indicating that AFO_o fault has occurred in the separator system.

In summary, the states of the separator, valve, and actuator for a period of 50 years are simulated using DMC, and the results are presented in Fig. 8. Then, the results of the DMC are input into the simulation model to obtain fault symptoms and simulation data. Fault symptoms are shown in Table 5. Next, fault symptoms are used to discretize the simulation data to obtain discrete data. Finally, Bayesian estimation is used to analyze the discrete dataset, resulting in parameters for the fault layer and the fault symptom layer. Table 6 shows the parameters of the fault layer nodes obtained based on DMC.

3.3.2. Parameter determination based on PM and SMC

3.3.2.1. PM and fuzzy theory introduction. Although the parameters of the fault symptom layer are confirmed based on SMC, this method has some drawbacks. Particularly, SMC can hardly simulate a situation where multiple faults occur simultaneously. This directly results in the inability to obtain complete CPTs for fault symptom layer nodes through analysis of discrete datasets based on SMC. Table 7 shows part of WL node's CPT. From this, it becomes evident that the scenario where the probabilities of all four states agree is not a result of calculations, but rather an approximation achieved by using the average value. Therefore, the CPTs of the fault symptom layer nodes are complemented by the introduction of PM and fuzzy theory.

A specific description of the PM used in this study can be found in subsection 2.2, and in this subsection only the fuzzy theory is explained. Wickens et al. (Chakraverty et al., 2019) suggests that the probability of an event can be divided into seven semantic values: very high, high, fairly high, moderate, fairly low, low, and very low. Their corresponding fuzzy numbers and λ -cut sets are shown in Table 8. The membership function is shown in Fig. 9. To accurately quantify the probability of events occurrences using fuzzy numbers, it is necessary to integrate the judgments of multiple PMs. The overall assessment results of n PMs can be calculated using (9):

$$\tilde{P}_i = \frac{\omega_1 f_{i1} \oplus \omega_2 f_{i2} \oplus \dots \oplus \omega_n f_{in}}{n} \quad i = 1, 2, \dots, m \quad j = 1, 2, \dots, n \quad (9)$$

Where, \tilde{P}_i represents the fuzzy occurrence probability of the i -th event, f_{ij} represents the fuzzy value assigned by the j -th PM to the i -th event, m represents the number of events, n represents the number of PMs and ω_i represents the weights of PMs.

Weight is often used to indicate the importance of something to an outcome. Due to the subjectivity and ambiguity in the description of an object by human experts, it is necessary to consider their education, work experience, age and other information when collecting their experience. Ultimately, this information is converted into weight that influence diagnostic results. Although PM is used to replace human experts, the decision of the j -th PM on the i -th event still affects the final diagnostic result through weights. But unlike human experts, PM has a high degree of objectivity and robustness to other factors because it is based on rigorous mathematical and physical formulas. Therefore, any calculation of the same PM will have the same impact on the final diagnostic results. Furthermore, it is assumed that there are n PMs, and when a failure occurs, their descriptions of the fault symptoms are also consistent. Due to the characteristics of PM, weight of each PM is made consistent in this study, i.e., $\omega_i = 1$.

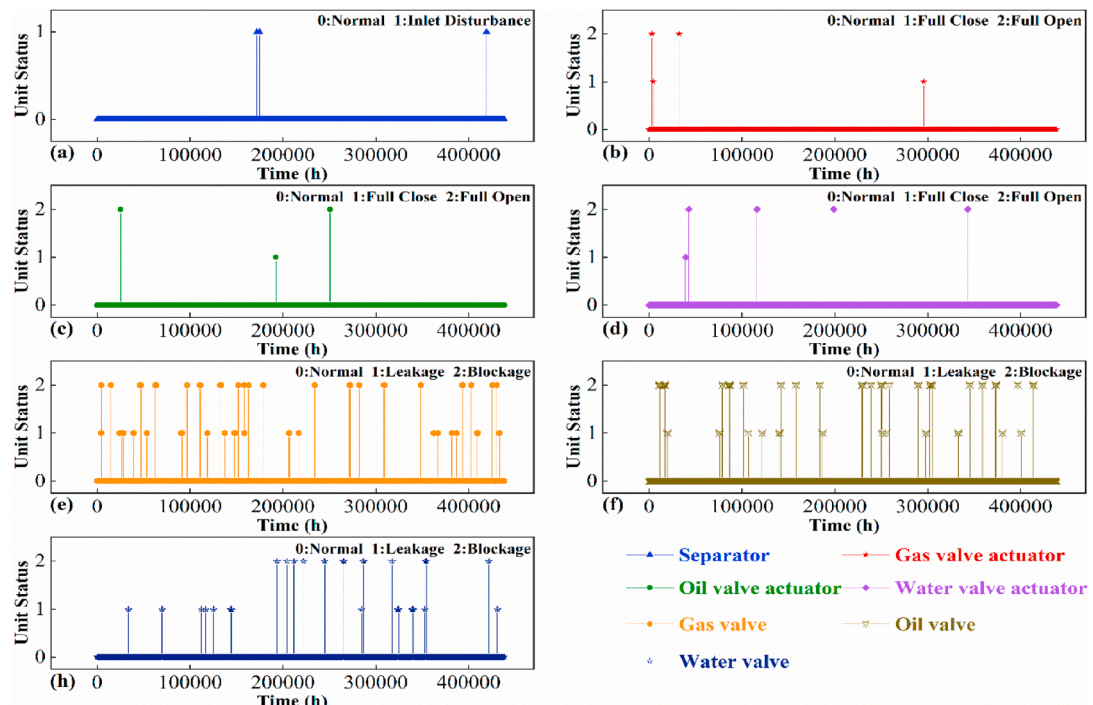


Fig. 8. DMC results. (a) Separator's result. (b) Gas valve PID actuator's result. (c) Oil valve PID actuator's result. (d) Water valve PID actuator's result. (e) Gas valve's result. (f) Oil valve's result. (g) Water valve's result.

Table 5
Fault symptoms.

Work States	Monitoring Parameters										
	WL	RIOL	RIIOL	VP	GVO	OVO	WVO	GOR	OOR	WOR	IF
$BLOCK_g$	N	N	N	H	H	L	L	L	L	L	L
$LEAK_g$	N	H	H	L	H	H	H	H	H	H	H
AFC_g	N	N	N	H	L	L	L	L	L	L	L
AFO_g	N	H	H	L	H	H	H	H	H	H	H
$BLOCK_w$	H	H	H	H	H	H	H	H	H	L	L
$LEAK_w$	L	L	L	N	L	L	H	L	L	H	H
AFC_w	H	H	H	H	H	H	L	H	L	L	L
AFO_w	L	L	L	L	L	L	H	L	H	H	H
$BLOCK_o$	N	H	H	H	H	H	L	H	L	L	L
$LEAK_o$	N	N	L	N	L	H	H	L	H	N	H
AFC_o	N	H	H	H	H	L	L	H	L	L	L
AFO_o	N	N	L	N	L	H	N	L	N	N	N
ID	S	N	S	S	S	S	S	S	S	S	S

Table 6
Fault layer parameters.

Node	States		Node	States	
	Absent (%)	Present (%)		Absent (%)	Present (%)
$BLOCK_g$	97.45	2.55	AFC_w	99.99	0.01
$LEAK_g$	98.03	1.97	AFO_w	99.93	0.07
$BLOCK_w$	99.07	0.93	AFC_o	99.95	0.05
$LEAK_w$	98.75	1.25	AFO_o	99.99	0.01
$BLOCK_o$	97.33	2.67	AFC_g	99.96	0.04
$LEAK_o$	99.20	0.80	AFO_g	99.95	0.05
ID	99.97	0.03			

After obtaining the fuzzy occurrence probability of the event through (9), it is necessary to perform a defuzzification (Chakraverty et al., 2019). In order to be consistent with the above fuzzy number λ cut set operation, the integral value method proposed by Liou et al. (Liou and Wang, 1992) is adopted in this paper, as shown in (10):

$$I(\tilde{P}) = (1 - \varepsilon)I_R(\tilde{P}) + \varepsilon I_L(\tilde{P}) \quad (10)$$

Where, $\varepsilon \in [0, 1]$ represents the optimism coefficient. When $\varepsilon = 0$ and $\varepsilon = 1$ are considered, $I(\tilde{P})$ represents the upper and lower bounds of the defuzzified value of the fuzzy number \tilde{P} . When $\varepsilon = 0.5$ is considered, $I(\tilde{P})$ represents the representative value of the defuzzified value of the fuzzy number \tilde{P} . $I_R(\tilde{P})$ and $I_L(\tilde{P})$ are the integral values of the inverse functions of the left and right membership functions of the fuzzy number, respectively.

For triangular fuzzy numbers and trapezoidal fuzzy numbers, $I_R(\tilde{P})$ and $I_L(\tilde{P})$ can be expressed using λ -cut sets, as shown in (11) and (12):

$$I_R(\tilde{P}) = \frac{1}{2} \left[\sum_{\lambda=0.1}^1 \lambda_R(\tilde{P}) \Delta \lambda + \sum_{\lambda=0}^{0.9} \lambda_R(\tilde{P}) \Delta \lambda \right] \quad (11)$$

$$I_L(\tilde{P}) = \frac{1}{2} \left[\sum_{\lambda=0.1}^1 \lambda_L(\tilde{P}) \Delta \lambda + \sum_{\lambda=0}^{0.9} \lambda_L(\tilde{P}) \Delta \lambda \right] \quad (12)$$

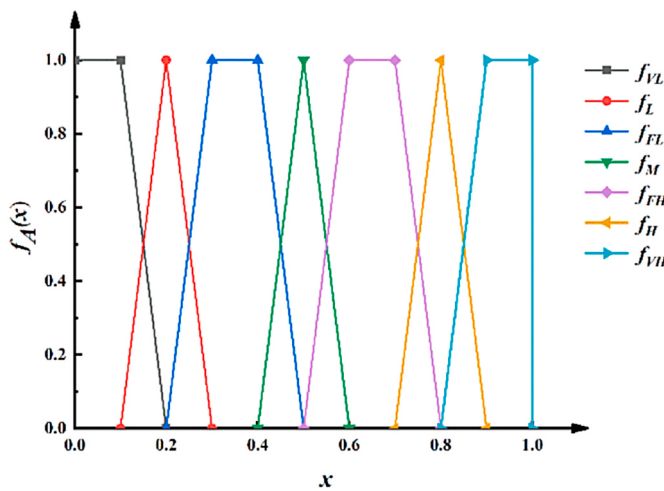
Table 7

Part of WL node's CPT.

Conditions						States			
AFO _w	AFO _o	AFO _g	AFC _w	AFC _o	AFC _g	N (%)	H (%)	L (%)	S (%)
Absent	Absent	Absent	Absent	Absent	Absent	99.999	0.0003	0.0003	0.0003
Absent	Absent	Absent	Absent	Present	Present	98.315	0.562	0.562	0.562
Absent	Absent	Absent	Absent	Present	Absent	98.592	0.469	0.469	0.469
Absent	Absent	Absent	Absent	Present	Present	25	25	25	25
Absent	Absent	Absent	Present	Absent	Absent	2.632	92.105	2.632	2.632
Absent	Absent	Absent	Present	Absent	Present	25	25	25	25
Absent	Absent	Absent	Present	Present	Absent	25	25	25	25
Absent	Absent	Absent	Present	Present	Present	25	25	25	25
Absent	Absent	Present	Absent	Absent	Absent	98.696	0.435	0.435	0.435
Absent	Absent	Present	Absent	Present	Present	25	25	25	25
Absent	Absent	Present	Absent	Present	Absent	25	25	25	25
Absent	Absent	Present	Absent	Present	Present	25	25	25	25

Table 8Fuzzy Numbers and λ -cut Set.

Fuzzy number	λ -cut set
$f_{VL} = (0, 0, 0.1, 0.2)$	$f_{VL}^{\lambda} = [0.1\lambda + 0, -0.1\lambda + 0.2]$
$f_L = (0.1, 0.2, 0.3)$	$f_L^{\lambda} = [0.1\lambda + 0.1, -0.1\lambda + 0.3]$
$f_{L} = (0.2, 0.3, 0.4, 0.5)$	$f_{L}^{\lambda} = [0.1\lambda + 0.2, -0.1\lambda + 0.5]$
$f_M = (0.4, 0.5, 0.6)$	$f_M^{\lambda} = [0.1\lambda + 0.4, -0.1\lambda + 0.6]$
$f_{FH} = (0.5, 0.6, 0.7, 0.8)$	$f_{FH}^{\lambda} = [0.1\lambda + 0.5, -0.1\lambda + 0.8]$
$f_H = (0.7, 0.8, 0.9)$	$f_H^{\lambda} = [0.1\lambda + 0.7, -0.1\lambda + 0.9]$
$f_{VH} = (0.8, 0.9, 1.0)$	$f_{VH}^{\lambda} = [0.1\lambda + 0.8, -0.1\lambda + 1.0]$

**Fig. 9.** Membership functions of fuzzy linguistic terms.

Where, $\lambda_R(\tilde{P})$ and $\lambda_L(\tilde{P})$ represent the upper and lower bounds of the λ -cut set of the fuzzy number \tilde{P} , respectively; $\lambda = 0, 0.1, 0.2, \dots, 1$; $\Delta\lambda = 0.1$.

3.3.2.2. PM and fuzzy theory application. Based on Subsection 3.3.2.1, the example of WOR node under $BLOCK_w$ fault is taken to demonstrate how PM and fuzzy theory can be employed to obtain parameters of the fault symptom layer: 1) Number of PMs is determined. In this example, 10 PMs are used for evaluation of fault symptoms in WOR nodes. 2) One PM is asked. Various faults are input into one PM to obtain a description of different fault symptoms by PM. This step is like asking one human expert. 3) Multiple PMs are asked. The boundary conditions of each PM are repeatedly changed to avoid the contingency of a single PM. In this way, it is possible to get fault symptoms in several dimensions. This step is like asking multiple human experts. 4) Semantics of PMs are obtained. It is found that by changing the boundary conditions of the PM several

times, when $BLOCK_w$ fault occurs in the separator, the flow rate behind its water valve decreases. Therefore, it can be concluded that when a $BLOCK_w$ fault occurs in the separator, the probability of the flow rate behind the water valve becoming lower is very high. Due to the complementarity, the likelihood of other phenomena occurring will be very low. In this example, the semantic evaluation of 10 PMs is shown in Table 9.

5) The average fuzzy number is determined. According to (9), the average fuzzy number for all states is shown in Table 10.

6) The defuzzification value of the fuzzy number is determined. This step is mainly done using (10), (11) and (12). In this example, the steps for solving the defuzzification of the average fuzzy number of Low state are shown below:

$$I_R(\tilde{P}) = \frac{1}{2} \times 0.1 \times (9.45 + 9.55) = 0.95 \quad (13)$$

$$I_L(\tilde{P}) = \frac{1}{2} \times 0.5 \times (8.55 + 8.45) = 0.85 \quad (14)$$

$$I(\tilde{P}) = 0.5 \times (0.95 + 0.85) = 0.9 \quad (15)$$

In summary, Normal, High and Shock defuzzification values are 0.125, 0.1 and 0.135 respectively. 7) The defuzzification values are converted to probability values. This step focuses on normalizing the defuzzification values to calculate the probability values for each state. Finally, the probability of each state of WOR node occurring when $BLOCK_w$ fault occurs is shown in Table 11.

In the above way, the characteristic description of PM on the flow rate behind the water valve can be obtained when each fault occurs independently. Then, (9)–(12) are used to convert the semantics into basic probability values, and the results are shown in Table 12. Finally, the Noisy-MAX(Díez and Galán, 2003) algorithm is used to obtain the WOR node's probability table provided by PM. The Noisy-MAX algorithm is shown in (16) and (17):

$$P(Y \leq y|X) = \prod_{i=1}^n \sum_{y'_i=0}^y q_{i,y_i}^{x_i} \quad (16)$$

$$P(Y=y|X) = \begin{cases} P(Y \leq 0|X) & \text{if } y=0, \\ P(Y \leq y|X) - P(Y \leq y-1|X) & \text{if } y > 0. \end{cases} \quad (17)$$

Where, X is the parent set of node Y , $X = x_1, x_2, \dots, x_n$, and $P(Y=0|X_1 = 0, \dots, X_n = 0) = 1$.

3.3.2.3. PM and SMC application. Based on the above, conditional probability table for each node in fault symptom layer can be obtained through PM and fuzzy theory. Then, CPTs obtained from SMC are

Table 9

Expert semantic results.

WOR States	PM Name									
	PM1	PM2	PM3	PM4	PM5	PM6	PM7	PM8	PM9	PM10
Normal	Very Low	Fairly Low	Very Low	Very Low						
High	Very Low	Very Low	Very Low							
Low	Very High	Very High	Very High							
Shock	Very Low	Very Low	Very Low	Very Low	Low	Very Low	Very Low	Very Low	Fairly Low	Very Low

Table 10

Average fuzzy number results.

WOR States	Average Fuzzy Number
Normal	[0.1λ + 0.02, - 0.1 + 0.23]
High	[0.1λ + 0, - 0.1λ + 0.2]
Low	[0.1λ + 0.8, - 0.1λ + 1.0]
Shock	[0.1λ + 0.03, - 0.1 + 0.24]

Table 11Probability of WOR node each state when $BLOCK_w$ fault occurs.

WOR States	Probability (%)
Normal	9.92
High	7.93
Low	71.42
Shock	10.71

merged with CPTs provided by PM to obtain final CPTs for nodes in fault symptom layer. Fig. 10 shows the specific process of fusing CPTs provided by SMC with CPTs provided by PM. Table 13 shows the result after filling the missing content in Table 7.

3.4. Diagnostic rules determination

BNs can use posterior probabilities and diagnostic rules to determine why the fault occurred. Therefore, following the relevant rules proposed by Cai et al. (Cai, n.d.; Cai et al., 2016b), the on-site engineer formulated the following diagnostic rules:

- 1) *Rule1*: If the difference between the posterior probability and the prior probability of the PRESENT state of a fault node is equal to or greater than 70%, a fault is reported.

- 2) *Rule2*: If the difference between the posterior probability and the prior probability of the PRESENT state of a fault node is greater than or equal to 30% and less than 70%, a warning is reported.
- 3) *Rule3*: If the difference between the posterior probability and the prior probability of the PRESENT state of a fault node is less than 30%, the system is operating normally.

To better understand the above rules, a case study is used for illustration. Suppose there are four fault nodes A, B, C and D. When fault symptoms are input into the model, the difference between the posterior probability and a priori probability of the PRESENT state of fault node A is 75%; the difference between the posterior probability and a priori probability of the PRESENT state of fault node B is 80%; the difference between the posterior probability and a priori probability of the PRESENT state of fault node C is 58% and the difference between the posterior probability and a priori probability of the PRESENT state of fault node D is 10%. Therefore, according to Rule 1, both fault A and fault B have occurred in the system; according to Rule 2, the system reports the warning of fault C, but the warning is not a fault; according to Rule 3, fault D has not occurred in the system.

4. Case study

In this section we first troubleshoot the horizontal three-phase separator in Section 2 using the methodology mentioned in Section 3 and analyze in detail three types of faults: $BLOCK_w$, AFC_w and ID . Secondly, to further validate the effectiveness of the model, the diagnostic results of BNs are not only compared with those of deep neural network (DNN), convolutional neural network (CNN), and deep residual network (RESNET), but the anti-noise interference capabilities of four models are also contrasted. Finally, the fault tolerance of the model is analyzed by the introduction of some inaccurate evidence into BNs.

Table 12

The WOR Node's basic probability.

ID	$LEAK_w$	$BLOCK_w$...	AFC_o	AFO_g	AFC_g	N(%)	H(%)	L(%)	S(%)
1	0	0	...	0	0	0	9.33	9.33	9.58	71.75
0	1	0	...	0	0	0	10.39	70.82	9.23	9.56
0	0	1	...	0	0	0	9.92	7.93	71.42	10.71
0	0	0	...	0	0	0	70.54	11.13	10.01	8.33
0	0	0	...	0	0	0	9.20	10.09	70.94	9.77
0	0	0	...	0	0	0	8.83	71.90	9.31	9.96
0	0	0	...	0	0	0	10.95	9.40	70.83	0.09
0	0	0	...	0	0	0	10.89	70.08	9.27	9.76
0	0	0	...	0	0	0	9.65	9.40	70.83	0.09
0	0	0	...	0	0	0	70.64	8.16	10.48	10.72
0	0	0	...	1	0	0	9.40	9.40	72.12	9.08
0	0	0	...	0	1	0	9.02	71.56	9.02	10.39
0	0	0	...	0	0	1	9.30	8.18	71.29	11.23

Annotation: 1 indicates the fault occurrence, 0 indicates no fault occurrence.

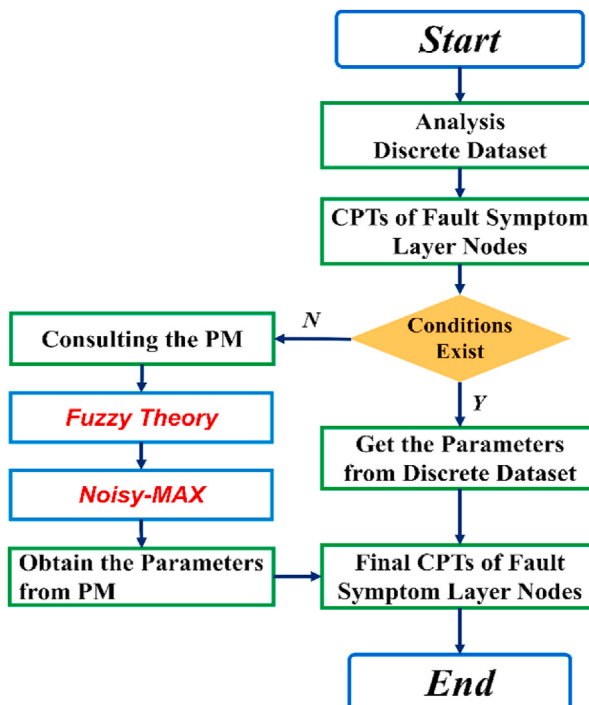


Fig. 10. Fault symptom layer parameter determination process.

4.1. Fault diagnosis case

4.1.1. Water valve blockage case

When the water valve in the separator becomes blocked, the flow behind the water valve suddenly becomes low. This reduces the inlet flow of separator. As the pressure inside the separator gradually increases due to the valve blockage, the level of each liquid phase inside the separator will show a gradual rising trend over time. Simultaneously, to reduce the pressure inside the separator, the opening of each valve is gradually increased under PID control. This results in a sudden increase in the flow rate of the oil and gas phase valves. These fault symptoms are fed into the model and the diagnostic results are shown in Fig. 11.

Fig. 11 shows that the probability of occurrence of the water valve blockage fault is close to 100%, while the probability of occurrence of the other faults is essentially 0. Therefore, according to Rule 1, it is judged that the water valve blockage fault has occurred in the separator system. This is consistent with the fault logs in the field.

4.1.2. Water valve actuator fully closed case

When the PID actuator of the water valve in the separator is fully

closed, the water valve of the separator is immediately closed, resulting in the flow rate behind the water valve gradually going to 0 and showing a downward trend. At the same time, the pressure inside the separator increases as the water valve is closed. Over time, the levels of the water and oil phases will increase. In addition, to reduce the pressure inside the separator, the opening of the gas and oil valves will gradually increase, so that the gas phase flow and the oil phase flow will also increase for a certain period. These fault symptoms are fed into the model and the diagnostic results are shown in Fig. 12.

Fig. 12 shows that the probability of a water valve actuator fully closed fault occurring is 94.4%, while other faults occur much less than it. Therefore, according to Rule 1, AFC_w fault may occur in the separator. This is consistent with the fault logs in the field.

4.1.3. Inlet disturbance case

Since the size of the separator system is relatively small, all monitored parameters are affected when the inlet is disturbed. By analyzing the field data, it is found that all parameters except RIOL exhibited oscillations. These fault symptoms are fed into the model and the diagnostic results are shown in Fig. 13.

Fig. 13 shows that the probability of the inlet disturbance fault occurring is 100%, while the probability of other faults occurring is much less than it. Therefore, according to Rule 1, the separator may have experienced an inlet disturbance fault. This is consistent with the fault logs in the field.

4.2. Models comparison

4.2.1. Accuracy comparison

BNs, DNN, CNN, and RESNET models are utilized to identify 14 operating states of the separator system, including normal states and 13 fault states. BNs is trained using the method proposed in this paper. The rest of the models complete their training using a dataset. The dataset consists of simulated data and field data provided by the field engineer. Meanwhile, to examine the training effect of BNs, DNN, CNN and RESNET, the dataset is divided into a training set and a test set, with a ratio of 7:3. The best performing models are chosen in the test set and are used for subsequent fault diagnosis. Finally, a completely new fault dataset is used to validate the diagnostic accuracy of all models. Again, it is emphasized that brand new data is not involved in the training of model. The parameter settings for DNN, CNN and RESNET models are shown in Table 14. They are all built with TENSORFLOW(Adabi et al., M et al.).

Fig. 14 illustrates the confusion matrix of four models, where the Y-axis of each subplot represents the true labels, and the X-axis represents the predicted labels. To facilitate a deeper understanding, AFC_g fault is taken as an example, and a detailed explanation of confusion matrix of BNs and CNN is provided. The confusion matrix of DNN and RESNET is like that of BNs and CNN, and much detail will not be delved into here.

Table 13
Results after filling in the missing parts of Table 7.

Conditions	States									
	AFO_w	AFO_o	AFO_g	AFC_w	AFC_o	AFC_g	N (%)	H (%)	L (%)	S (%)
Absent	Absent	Absent	Absent	Absent	Absent	Absent	99.99	0.0003	0.0003	0.0003
Absent	Absent	Absent	Absent	Absent	Present	98.315	0.562	0.562	0.562	0.562
Absent	Absent	Absent	Absent	Present	Absent	98.592	0.469	0.469	0.469	0.469
Absent	Absent	Absent	Absent	Present	Present	50.87	13.866	17.083	18.181	18.181
Absent	Absent	Absent	Present	Absent	Absent	2.632	92.105	2.632	2.632	2.632
Absent	Absent	Absent	Present	Absent	Present	51.101	14.291	15.699	18.909	18.909
Absent	Absent	Absent	Present	Present	Absent	51.068	14.189	16.237	18.506	18.506
Absent	Absent	Absent	Present	Present	Present	36.435	16.124	20.973	26.468	26.468
Absent	Absent	Present	Absent	Absent	Absent	98.696	0.435	0.435	0.435	0.435
Absent	Absent	Present	Absent	Absent	Present	52.329	13.545	16.065	18.061	18.061
Absent	Absent	Present	Absent	Present	Absent	52.295	13.443	16.608	17.654	17.654
Absent	Absent	Present	Absent	Present	Present	37.31	15.636	21.354	25.699	25.699

Table 14
DNN, CNN and RESNET model parameters.

Models	Parameters	Function/Value
DNN	Number of hidden layers	3
	Activation function of hidden layer	Relu; Relu; Relu
	Number of neurons in hidden layer	$16 \times 16 \times 16$
	Number of batch normalization layers	3
	Activation function of output layer	Softmax
	Optimizer	Adam
	Learning rate	0.001
	Epochs	500
	Number of convolutional layers	3
	Activation function of convolutional layer	Relu; Relu; Relu
CNN	Number of filters in convolutional layer	$32 \times 32 \times 32$
	Convolutional kernel size of convolutional layer	$2 \times 2 \times 2$
	Number of maxpooling layers	2
	Size of kernel in maxpooling layer	2×2
	Size of stride in maxpooling layer	2×2
	Setting of padding in maxpooling layer	Same; Same
	Number of batch normalization layers	1
	Number of flatten layers	1
	Activation function of output layer	Softmax
	Optimizer	Adam
RESNET	Learning rate	0.001
	Epochs	500
	Number of resblock layers	2
	Number of filters in resblock layer	32×32
	Size of kernel in resblock layer	4×4
	Number of basicblock layers	1
	Size of filters in basicblock layer	32
	Size of kernel in basicblock layer	4
	Size of stride in basicblock layer	2
	Setting of padding in basicblock layer	Same

Fig. 14(a) shows that when diagnosing AFC_g fault, BNs considers the probability of this fault being a AFC_g fault as 98.9%, the probability of it being a $LEAK_g$ fault as 0.2%, and the probability of it being a $BLOCK_g$ fault as 1.5%. Therefore, AFC_g fault is accurately identified by BNs. Simultaneously, Fig. 14(b) shows that when diagnosing AFC_g fault, CNN considers the probability of this fault being a AFC_g fault as 100%. Furthermore, CNN does not misclassify AFC_g faults as other faults. Therefore, AFC_g fault is also accurately identified by CNN. Through the above analysis, on the new fault dataset, it can be found that the accuracy of BNs is 100%, while the accuracy of DNN, CNN and RESNET models are 91.34%, 87.99% and 94.62%, respectively. It can be concluded that our proposed model has a high diagnostic accuracy compared to some deep learning models.

4.2.2. Robustness comparison

Signal-to-noise ratio (SNR) is a measure of the proportionality between signal and noise, the higher value of the SNR, the higher power or energy of signal relative to the noise and the better signal quality. Therefore, SNR can be used as a measure of the quality of the signal affected by noise. In this subsection, the diagnostic capabilities of four models are tested for different faults at 10 db, 20 db, 30 db, 40 db and 50 db to investigate the robustness of each model. To better illustrate the extent to which different SNRs affect the data, some results of comparison are plotted as shown in Fig. 15. As mentioned above, the higher SNR, the less data is disturbed by noise. Fig. 16 shows the diagnostic capability of four models for different faults at different SNRs.

It can be seen from Fig. 16 that as the SNR increases, the recognition accuracy of BNs for various faults gradually improves and tends to 100%. Although the diagnostic accuracy of other models for different faults improves with increasing SNR, there are still cases of low detection accuracy. For example, at 50 db, CNN has a very low diagnostic accuracy for AFO_o fault. In addition, the diagnostic accuracy of BNs for various faults is almost better than other models at the same SNR, although the diagnostic accuracy of BNs for some faults is not very high in the 10 db case. In summary, our proposed model has strong robustness compared to some deep learning models.

4.3. Fault-tolerance test

To verify the fault tolerance of the proposed model, 2–3 error evidence is randomly input. Moreover, the BNs model will also be trained using two methods to make the results more convincing. The first method is the training approach proposed in this paper. The second approach uses a dataset to train the BNs model. This dataset is a discrete dataset consisting of simulation results of DMC and fault symptoms. Due to the large number of combinations of randomly selecting 2–3 nodes from 11 nodes, it is impossible to list all the analysis results in the paper. In this study, therefore, four cases are analyzed in detail.

4.3.1. Case 1

In case 1, incorrect evidence is entered for each output flow, and the diagnostic results for both models are shown in Fig. 17(a). It is found that the proposed BNs diagnose $BLOCK_w$ as AFC_w , $LEAK_o$ as AFO_o , $LEAK_g$ as AFO_g , $BLOCK_o$ as $BLOCK_g$, and AFC_o as $BLOCK_g$. It is considered acceptable that $BLOCK_w$ is diagnosed as AFC_w , $LEAK_o$ as AFO_o , and $LEAK_g$ as AFO_g . This is because even if there is an error in the evidence input, the model can still accurately diagnose the location of fault in the system. For example, both $BLOCK_w$ and AFC_w indicate that the water valve has failed. In summary, the proposed BNs successfully diagnosed 11 faults in this case with a diagnostic accuracy of 84.6%. However, the data-trained BNs successfully diagnosed 4 faults in this case with a diagnostic accuracy of 30.8%.

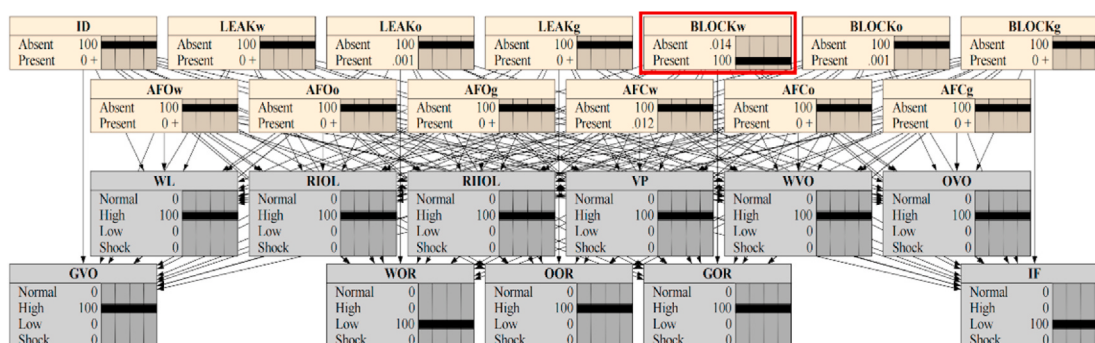


Fig. 11. $BLOCK_w$ diagnosis result.

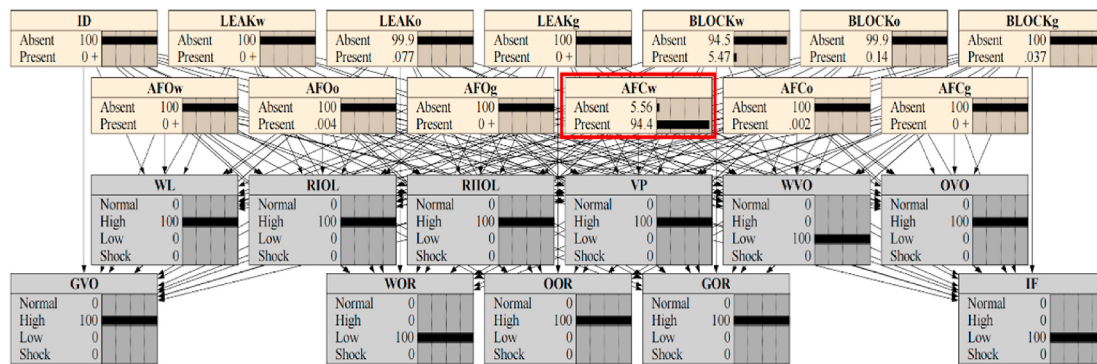
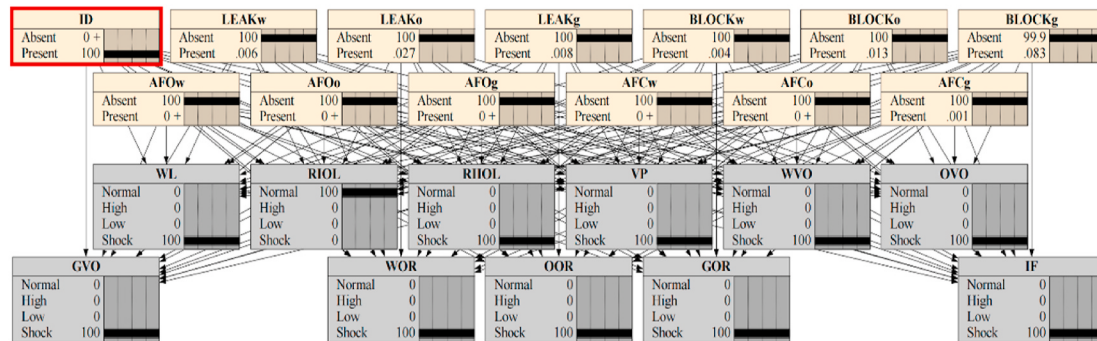
Fig. 12. AFC_w diagnosis result.

Fig. 13. ID diagnosis result.

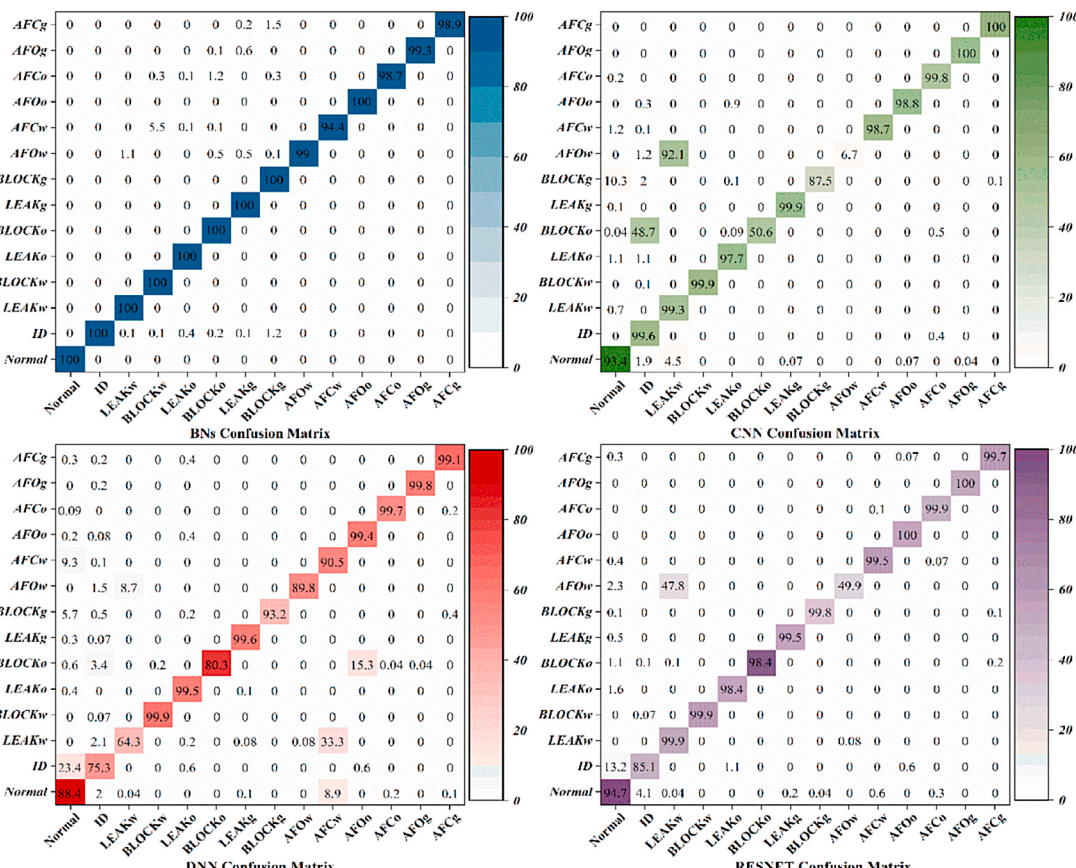


Fig. 14. Confusion matrix of four models. (a) BNs confusion matrix. (b) CNN confusion matrix. (c) DNN confusion matrix. (d) RESNET confusion matrix.

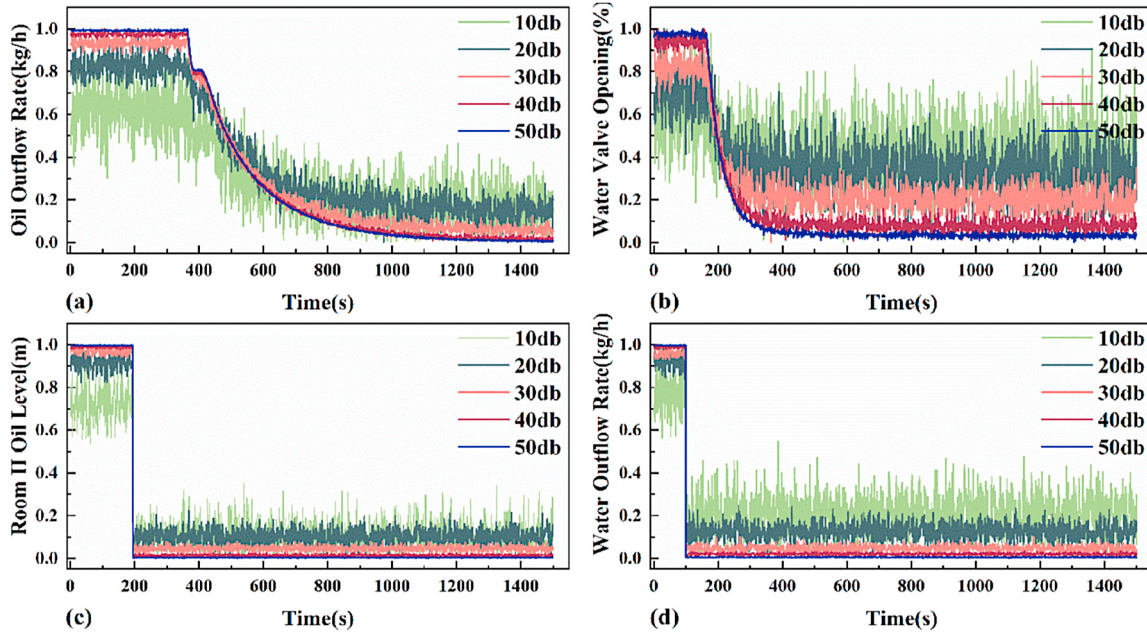


Fig. 15. Different SNRs comparison results. (a) $BLOCK_g$ fault's oil outflow rate. (b) $BLOCK_o$ fault's water valve opening. (c) $LEAK_o$ fault's Room II oil level. (d) $BLOCK_w$ fault's water outflow rate.

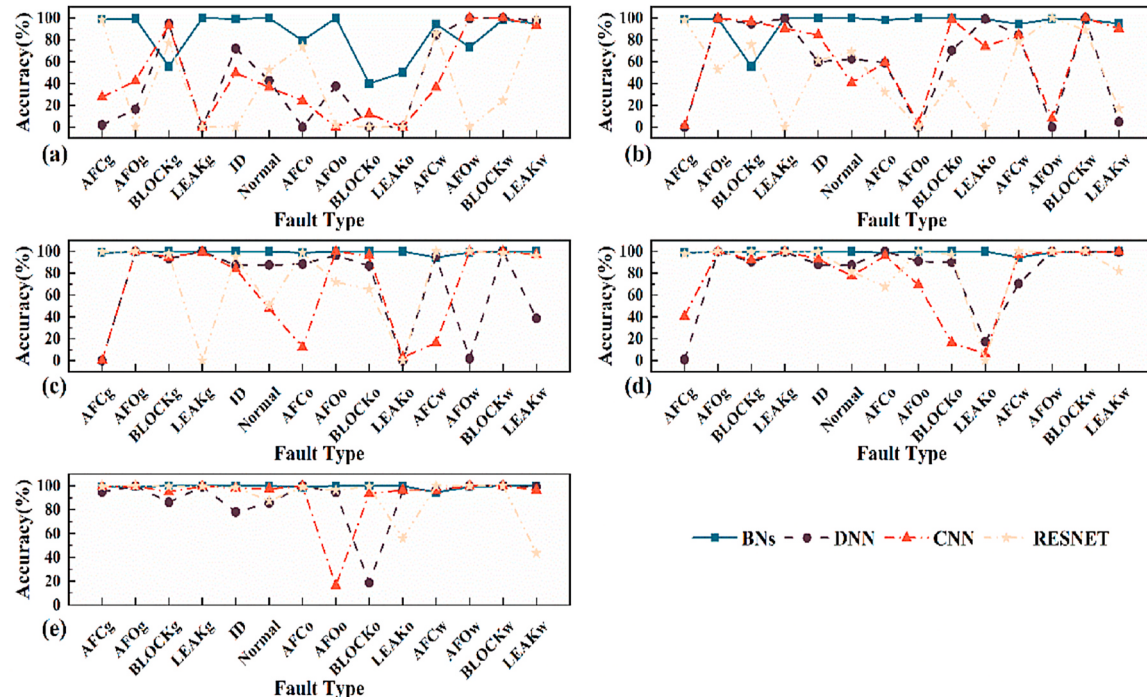


Fig. 16. Diagnostic accuracy of each model for different faults at different SNRs. (a) SNR is 10 db. (b) SNR is 20 db. (c) SNR is 30 db. (d) SNR is 40 db. (e) SNR is 50 db.

4.3.2. Case 2

In case 2, incorrect evidence for each valve opening is entered, and the diagnostic results for both models are shown in Fig. 17(b). It is found that the proposed BNs diagnose $BLOCK_w$ as AFC_w , $BLOCK_o$ as AFC_o , $LEAK_o$ as AFO_o , $BLOCK_g$ as AFC_g , and $LEAK_g$ as $BLOCK_o$. In summary, the proposed BNs successfully diagnosed 12 faults in this case with a diagnostic accuracy of 92.3%. However, the data-trained BNs successfully diagnosed 4 faults in this case with a diagnostic accuracy of 30.8%.

4.3.3. Case 3

In case 3, incorrect evidence for gas valve flow rate and inlet flow is entered, and the diagnostic results for both models are shown in Fig. 17(c). It is found that the proposed BNs diagnose $BLOCK_w$ as AFC_w , and $LEAK_g$ as $BLOCK_o$. In summary, the proposed BNs successfully diagnoses 12 faults in this case with a diagnostic accuracy of 92.3%. However, the data-trained BNs successfully diagnoses 7 faults in this case with a diagnostic accuracy of 53.8%.

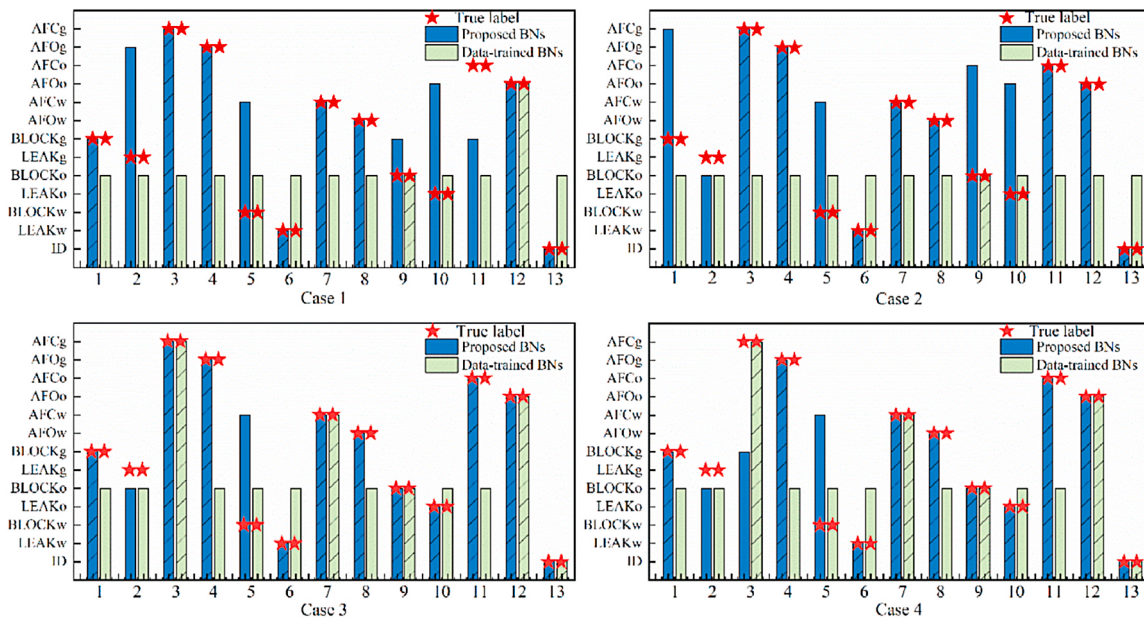


Fig. 17. Model comparison results. (a) Case 1. (b) Case 2. (c) Case 3. (d) Case 4.

4.3.4. Case 4

In case 4, incorrect evidence for room II oil level and inlet flow is entered, and the diagnostic results for both models are shown in Fig. 17(d). It is found that the proposed BNs diagnose $BLOCK_w$ as AFC_w , $LEAK_g$ as $BLOCK_o$ and AFC_g as $BLOCK_g$. In summary, the proposed BNs successfully diagnosed 12 faults in this case with a diagnostic accuracy of 92.3%. However, the data-trained BNs successfully diagnosed 7 faults in this case with a diagnostic accuracy of 53.8%.

From the above four cases, it can be concluded that the proposed BNs are more fault-tolerant than the data-trained BNs when there are 2~3 errors in the evidence. Of course, from the above analysis, it can also be concluded that misjudgments may be experienced by the proposed model when there is error evidence, and the specific reasons can be divided into two aspects:

- 1) *Fault Symptoms Lead to Misdiagnosis.* The BNs model accomplishes fault diagnosis by inputting fault symptoms and then updating the posterior probabilities using an inference algorithm. Therefore, when there is evidence of an input error, it may cause the symptoms of this fault to be similar to those of other faults. In this study, there are a total of 11 fault symptom nodes. Therefore, in case 1, when each output flow evidence is entered incorrectly, 5 of $LEAK_o$'s fault symptoms are the same as AFO_o 's, with a 45.4% similarity in failure symptoms; 5 of $LEAK_g$'s fault symptoms are the same as AFO_g 's, with a 45.4% similarity in fault symptoms; 8 of $BLOCK_w$'s fault symptoms are the same as AFC_w 's, with a 72.7% similarity in fault symptoms. As a result, this can lead to misdiagnosis in BNs. Ultimately, this is related to the fact that Bayesian networks are not good at extracting deep features. The subsequent solution is to add the critical process parameters or to perform feature extraction on the data and then use Bayesian networks for further fault identification.
- 2) *Noisy-MAX Model Lead to Misdiagnosis.* Although the Noisy-MAX model can simplify the CPT construction process, it has certain drawbacks. First, there is an independence assumption in the Noisy-MAX model, i.e. the occurrence of symptom Y due to cause X_i is independent of the occurrence of symptom Y due to cause X_j ($i \neq j$) (Li et al., 2011). Second, the ordering of node states when constructing node CPTs using the Noisy-MAX model also affects the CPTs (Zagorecki and Drudzel, 2013). Both are defective properties inherent in the Noisy-MAX model itself, which we cannot avoid. To diminish its impact, the physical models can be used to simulate

more operating states, thereby expanding the fault database. It will reduce the number of times the Noisy-MAX model is used and increase the accuracy of the model.

In summary, the fact that the proposed model is subject to misdiagnosis may be a deficiency of the model itself rather than a deficiency of the study.

5. Conclusions

In this paper, a Bayesian network fault diagnosis model based on SMC and PM is designed for a horizontal three-phase separator in an offshore crude oil treatment system. The main role of BNs is to be used to locate the faults and to intuitively explain the causes of faults. The main role of the SMC is to provide training data to the BNs to compensate for the lack of fault data in the field. PM not only overcomes the shortcomings of SMC and provide missing parameters to BNs, but also replaces the work of human experts, provides more accurate fault symptoms, and improves the accuracy and fault tolerance of the model. Finally, 13 faults in the separator system have been successfully diagnosed using this method, and $BLOCK_w$, AFC_w and ID have been analyzed in detail:

- 1) *Case 1:* When the separator water valve is blocked, the posterior probability of $BLOCK_w$ node failure state in the model changes from 0.93% to 100%.
- 2) *Case 2:* When the separator water valve actuator is fully closed, the posterior probability of AFC_w node failure state in the model changes from 0.01% to 94.4%.
- 3) *Case 3:* When the inlet of the separator is disturbed, the posterior probability of ID node failure state in the model changes from 0.03% to 100%.

Meanwhile, the proposed model is compared with DNN, CNN, and RESNET models. The results show that the diagnostic accuracy of the proposed model is 100%, while the diagnostic accuracies of DNN, CNN and RESNET models are 91.34%, 87.99% and 94.62% respectively. Therefore, it is proved that the proposed model is accurate and effective. Then, the robustness of four models is compared at different SNRs. Comparison results show that proposed method has better diagnostic accuracy than DNN, CNN and RESNET for all types of faults at different

SNRs. Moreover, with the increase of SNR, the diagnostic accuracy of the proposed model for various faults continues to improve and tends to 100%, while low-accuracy cases still occur in DNN, CNN, and RESNET. Therefore, results show that proposed model has good noise immunity. Finally, the proposed model is compared with the data-trained BNs. The results show that the proposed model is better than the data-trained BNs when there are 2~3 evidence input errors. Therefore, it further proves that the proposed model has better fault tolerance compared to the data-trained BNs.

However, the proposed model still has shortcomings, such as the possibility of misdiagnosis when a small amount of evidence is input incorrectly. In addition, the method has only been used in a small system such as a separator and has not been further tested in a large system. Consequently, the proposed method can be further researched and improved for wider dissemination and use to verify its effectiveness.

CRediT authorship contribution statement

Daqian Liu: Software, Methodology, Data curation, Conceptualization, Writing-original draft, Writing-revised draft. **Shangfei Song:** Writing-original draft, Methodology, Conceptualization, Writing-revised draft. **Ting Huang:** Validation, Investigation. **Siheng Shen:** Software, Investigation, Data curation. **Xiaoping Li:** Supervision, Project administration. **Jing Gong:** Supervision, Funding acquisition, Conceptualization.

Declaration of competing interest

The authors declare that they have no known competing financial interests or personal relationships that could have appeared to influence the work reported in this paper.

Data availability

Data will be made available on request.

Acknowledgment

This work is supported by the National Natural Science Foundation of China [Grand numbers: 52104069]; Beijing Municipal Natural Science Foundation [Grand number: 3232030]; the National Key Research and Development Program of China [Grand number: 2022YFC2806200]; China Postdoctoral Science Foundation [Grand number: 2022M713460]; Science Foundation of China University of Petroleum, Beijing [Grand number: 2462023BJRC018], all of which are gratefully acknowledged.

References

- Abadi, M., Barham, P., Chen, J., Chen, Z., Davis, A., Dean, J., Devin, M., Ghemawat, S., Irving, G., Isard, M., Kudlur, M., Levenberg, J., Monga, R., Moore, S., Murray, D.G., Steiner, B., Tucker, P., Vasudevan, V., Warden, P., Wicke, M., Yu, Y., Zheng, X., n.d. TensorFlow: A System for Large-Scale Machine Learning.
- Abdelhafidh, M., Fourati, M., Chaari, L., 2023. Dynamic Bayesian network-based operational risk assessment for industrial water pipeline leakage. *Comput. Ind. Eng.* 183, 109466. <https://doi.org/10.1016/j.cie.2023.109466>.
- Ahmad, S., Ahmad, Z., Kim, J.-M., 2022. A Centrifugal Pump Fault Diagnosis Framework Based on Supervised Contrastive Learning, vol. 15.
- Alves, I.M., Miranda, V., Carvalho, L.M., 2020. Parallel GPU Implementation for Fast generating system adequacy assessment via sequential Monte Carlo simulation. In: 2020 International Conference on Probabilistic Methods Applied to Power Systems (PMAPS).
- Amin, MdT., Khan, F., Imtiaz, S., 2018. Dynamic availability assessment of safety critical systems using a dynamic Bayesian network. *Reliab. Eng. Syst. Saf.* 178, 108–117. <https://doi.org/10.1016/j.ress.2018.05.017>.
- An, Q.-T., Sun, L.-Z., Zhao, K., Sun, L., 2011. Switching Function Model-Based Fast-Diagnostic Method of Open-Switch Faults in Inverters Without Sensors. *IEEE Transactions on Power Electronics* 26, 119–126. <https://doi.org/10.1109/TPEL.2010.2052472>.
- Askarian, M., Zarghami, R., Jalali-Farahani, F., Mostoufi, N., 2016. Fusion of micro-macro data for fault diagnosis of a sweetening unit using Bayesian network. *Chemical Engineering Research and Design*, 10th European Congress of Chemical Engineering 115, 325–334. <https://doi.org/10.1016/j.cherd.2016.09.008>.
- Bartlett, L.M., Hurdle, E.E., Kelly, E.M., 2009. Integrated system fault diagnostics utilising digraph and fault tree-based approaches. *Reliab. Eng. Syst. Saf.* 94, 1107–1115. <https://doi.org/10.1016/j.ress.2008.12.005>.
- Bouejla, A., Chaze, X., Guarneri, F., Napoli, A., 2014. A Bayesian network to manage risks of maritime piracy against offshore oil fields. *Saf. Sci.* 68, 222–230. <https://doi.org/10.1016/j.ssci.2014.04.010>.
- Cai, B., n.d. A Dynamic-Bayesian-Network-Based Fault Diagnosis Methodology Considering Transient and Intermittent Faults | IEEE Journals & Magazine | IEEE Xplore [WWW Document]. URL <https://ieeexplore.ieee.org/document/7495018> (accessed 7.6.23).
- Cai, B., Liu, Y., Fan, Q., Zhang, Y., Liu, Z., Yu, S., Ji, R., 2014. Multi-source information fusion based fault diagnosis of ground-source heat pump using Bayesian network. *Appl. Energy* 114, 1–9. <https://doi.org/10.1016/j.apenergy.2013.09.043>.
- Cai, B., Liu, Y., Ma, Y., Liu, Z., Zhou, Y., Sun, J., 2015. Real-time reliability evaluation methodology based on dynamic Bayesian networks: a case study of a subsea pipe ram BOP system. *ISA (Instrum. Soc. Am.) Trans.* 58, 595–604. <https://doi.org/10.1016/j.isatra.2015.06.011>.
- Cai, B., Liu, H., Xie, M., 2016a. A real-time fault diagnosis methodology of complex systems using object-oriented Bayesian networks. *Mech. Syst. Signal Process.* 80, 31–44. <https://doi.org/10.1016/j.ymssp.2016.04.019>.
- Cai, B., Zhao, Y., Liu, H., Xie, M., 2016b. A data-driven Fault Diagnosis methodology in three-phase inverters for PMSM drive systems. *IEEE Trans. Power Electron.* 1. <https://doi.org/10.1109/TPEL.2016.2608842>, 1.
- Calixto, E., 2016. Chapter 1 - lifetime data analysis. In: Calixto, E. (Ed.), *Gas and Oil Reliability Engineering*, second ed. Gulf Professional Publishing, Boston, pp. 1–92. <https://doi.org/10.1016/B978-0-12-805427-7.00001-4>.
- Chakraverty, S., Sahoo, D.M., Mahato, N.R., 2019. Defuzzification. In: Chakraverty, S., Sahoo, D.M., Mahato, N.R. (Eds.), *Concepts of Soft Computing: Fuzzy and ANN with Programming*. Springer, Singapore, pp. 117–127. https://doi.org/10.1007/978-981-13-7430-2_7.
- Cheliotis, M., Lazakis, I., Theotokatos, G., 2020. Machine learning and data-driven fault detection for ship systems operations. *Ocean Engineering* 216, 107968. <https://doi.org/10.1016/j.oceaneng.2020.107968>.
- Chen, X., Duan, Y., Houthooft, R., Schulman, J., Sutskever, I., Abbeel, P., InfoGAN: Interpretable Representation Learning by Information Maximizing Generative Adversarial Nets. <https://doi.org/10.48550/arXiv.1606.03657>.
- Cheng, Q., Wang, S., Yan, C., 2017. Sequential Monte Carlo simulation for robust optimal design of cooling water system with quantified uncertainty and reliability. *Energy* 118, 489–501. <https://doi.org/10.1016/j.energy.2016.10.051>.
- Dai, X., Gao, Z., 2013. From model, signal to knowledge: a data-driven perspective of fault detection and diagnosis. *IEEE Trans. Ind. Inf.* 9, 2226–2238. <https://doi.org/10.1109/TII.2013.2243743>.
- Díez, F.J., Galán, S.F., 2003. Efficient computation for the noisy MAX: computation for the Noisy MAX. *Int. J. Intell. Syst.* 18, 165–177. <https://doi.org/10.1002/int.10080>.
- Du, Z., Chen, L., Jin, X., 2017. Data-driven based reliability evaluation for measurements of sensors in a vapor compression system. *Energy* 122, 237–248. <https://doi.org/10.1016/j.energy.2017.01.055>.
- Feng, Z., Ma, H., Zuo, M.J., 2017. Spectral negentropy based sidebands and demodulation analysis for planet bearing fault diagnosis. *Journal of Sound and Vibration* 410, 124–150. <https://doi.org/10.1016/j.jsv.2017.08.024>.
- Fernandez-de-Cossio-Díaz, J., Vazquez, A., 2018. A physical model of cell metabolism. *Sci. Rep.* 8, 8349. <https://doi.org/10.1038/s41598-018-26724-7>.
- Ferreiro, S., Arnaiz, A., Sierra, B., Irigoien, I., 2012. Application of bayesian networks in prognostics for a new integrated vehicle health management concept. *Expert Syst. Appl.* 39, 6402–6418. <https://doi.org/10.1016/j.eswa.2011.12.027>.
- Figuerola Barraza, J., López Drogueyt, E., Ramos Martins, M., 2024. FS-SCF network: Neural network interpretability based on counterfactual generation and feature selection for fault diagnosis. *Expert Systems with Applications* 237, 121670. <https://doi.org/10.1016/j.eswa.2023.121670>.
- Gjerstad, T., 1985. *OREDA - the Reliability Data Reference for the Offshore Industry*.
- Goodfellow, I., Pouget-Abadie, J., Mirza, M., Xu, B., Warde-Farley, D., Ozair, S., Courville, A., Bengio, Y., 2014. Generative Adversarial Networks. *Advances in Neural Information Processing Systems* 3. <https://doi.org/10.1145/3422622>.
- Gramling, R., Freudenburg, W.R., 2006. Attitudes toward offshore oil development: a summary of current evidence. *Ocean Coast Manag.* 49, 442–461. <https://doi.org/10.1016/j.ocecoaman.2006.03.010>.
- Grezmak, J., Zhang, J., Wang, P., Loparo, K.A., Gao, R.X., 2020. Interpretable Convolutional Neural Network Through Layer-wise Relevance Propagation for Machine Fault Diagnosis. *IEEE Sensors Journal* 20, 3172–3181. <https://doi.org/10.1109/JSEN.2019.2958787>.
- Gribaudo, M., Iacono, M., Marrone, S., 2015. Exploiting bayesian networks for the analysis of combined attack trees. *Electronic notes in theoretical computer science. Proceedings of the Seventh International Workshop on the Practical Application of Stochastic Modelling (PASM)* 310, 91–111. <https://doi.org/10.1016/j.entcs.2014.12.014>.
- Guo, J., Si, Z., Xiang, J., 2022. A compound fault diagnosis method of rolling bearing based on wavelet scattering transform and improved soft threshold denoising algorithm. *Measurement* 196, 111276. <https://doi.org/10.1016/j.measurement.2022.111276>.
- Handel, A., La Gruta, N.L., Thomas, P.G., 2020. Simulation modelling for immunologists. *Nat. Rev. Immunol.* 20, 186–195. <https://doi.org/10.1038/s41577-019-0235-3>.
- Hasan, M.J., Rai, A., Ahmad, Z., Kim, J.-M., 2021. A Fault Diagnosis framework for centrifugal pumps by scalogram-based imaging and deep learning. *IEEE Access* 9, 58052–58066. <https://doi.org/10.1109/ACCESS.2021.3072854>.

- Hou, L., Wu, X., Wu, Z., Wu, S., 2020. Pattern identification and risk prediction of domino effect based on data mining methods for accidents occurred in the tank farm. Reliab. Eng. Syst. Saf. 193, 106646. <https://doi.org/10.1016/j.ress.2019.106646>.
- Hu, J., Sun, J., Bian, C., Tong, J., Xia, S., 2013. Electrodeposition of three-dimensional (3D) Ag/Pd bimetallic nanodendrites and application for total nitrogen determination. Key Eng. Mater. 562–565, 652–657. <https://doi.org/10.4028/www.scientific.net/KEM.562-565.652>.
- Huang, Y., McMurran, R., Dhadialla, G., Peter Jones, R., 2008. Probability based vehicle fault diagnosis: bayesian network method. J. Intell. Manuf. 19, 301–311. <https://doi.org/10.1007/s10845-008-0083-7>.
- Huang, Y., Cai, J., Dai, D., 2020. Fault diagnosis of RAT actuator based on bayesian network. In: 2020 IEEE 2nd International Conference on Civil Aviation Safety and Information Technology (ICCASIT). Presented at the 2020 IEEE 2nd International Conference on Civil Aviation Safety and Information Technology (ICCASIT), IEEE, Weihai, China, pp. 859–863. <https://doi.org/10.1109/ICCASIT50869.2020.9368662>.
- Jeffreys, H., n.d. XXVIII. On some criticisms of the theory of probability: London, Edinburgh Dublin Phil. Mag. J. Sci.: Vol 22, No 146 [WWW Document]. URL <https://www.tandfonline.com/doi/abs/10.1080/14786443608561691> (accessed 7.8.23).
- Indrawan, N., Shadie, L.J., Breault, R.W., Panday, R., Chitnis, U.K., 2021. Data analytics for lead detection in a subcritical boiler. Energy 220, 119667. <https://doi.org/10.1016/j.energy.2020.119667>.
- Jiao, J., Zhao, M., Lin, J., Liang, K., 2019. Hierarchical discriminating sparse coding for weak fault feature extraction of rolling bearings. Reliability Engineering & System Safety, Impact of Prognostics and Health Management in Systems Reliability and Maintenance Planning 184, 41–54. <https://doi.org/10.1016/j.ress.2018.02.010>.
- Jing, Y., 2022. Fault diagnosis of landing gear extension and retraction system based on fuzzy Fault tree and bayesian network. In: 2022 IEEE 4th International Conference on Civil Aviation Safety and Information Technology (ICCASIT). Presented at the 2022 IEEE 4th International Conference on Civil Aviation Safety and Information Technology (ICCASIT), IEEE, Dali, China, pp. 644–647. <https://doi.org/10.1109/ICCASIT55263.2022.9986573>.
- Kellil, N., Aissat, A., Mellit, A., 2023. Fault diagnosis of photovoltaic modules using deep neural networks and infrared images under Algerian climatic conditions. Energy 263, 125902. <https://doi.org/10.1016/j.energy.2022.125902>.
- Khakzad, N., Khan, F., Amyotte, P., 2011. Safety analysis in process facilities: comparison of fault tree and Bayesian network approaches. Reliab. Eng. Syst. Saf. 96, 925–932. <https://doi.org/10.1016/j.ress.2011.03.012>.
- Khaled, M.S., Imtiaz, S., Ahmed, S., Zendehboudi, S., 2021. Dynamic simulation of offshore gas processing plant for normal and abnormal operations. Chem. Eng. Sci. 230, 116159. <https://doi.org/10.1016/j.ces.2020.116159>.
- Kong, X., Cai, B., Khan, J.A., Gao, L., Yang, J., Wang, B., Yu, Y., Liu, Y., 2024. Concurrent fault diagnosis method for electric-hydraulic system: subsea blowout preventer system as a case study. Ocean. Eng. 294, 116818. <https://doi.org/10.1016/j.oceaneng.2024.116818>.
- Labeau, P.E., Zio, E., 2002. Procedures of Monte Carlo transport simulation for applications in system engineering. Reliab. Eng. Syst. Saf. 77, 217–228. [https://doi.org/10.1016/S0951-8320\(02\)00055-8](https://doi.org/10.1016/S0951-8320(02)00055-8).
- Li, Y., O'Neill, Z., 2018. A critical review of fault modeling of HVAC systems in buildings. Build. Simulat. 11, 953–975. <https://doi.org/10.1007/s12273-018-0458-4>.
- Li, W., Poupart, P., van Beek, P., 2011. Exploiting structure in weighted model counting approaches to probabilistic inference. JAIR 40, 729–765. <https://doi.org/10.1613/jair.3232>.
- Li, X., Gong, C., Gu, L., Jing, Z., Fang, H., Gao, R., 2019. A reliability-based optimization method using sequential surrogate model and Monte Carlo simulation. Struct. Multidiscip. Optim. 59, 439–460. <https://doi.org/10.1007/s00158-018-2075-3>.
- Li, T., Zhou, Y., Zhao, Y., Zhang, C., Zhang, X., 2022. A hierarchical object oriented Bayesian network-based fault diagnosis method for building energy systems. Appl. Energy 306, 118088. <https://doi.org/10.1016/j.apenergy.2021.118088>.
- Lin, M., Li, J., Li, Y., Wang, X., Jin, C., Chen, J., 2023. Generalization analysis and improvement of CNN-based nuclear power plant fault diagnosis model under varying power levels. Energy 282, 128905. <https://doi.org/10.1016/j.energy.2023.128905>.
- Liou, T.-S., Wang, M.-J.J., 1992. Ranking fuzzy numbers with integral value. Fuzzy Set Syst. 50, 247–255. [https://doi.org/10.1016/0165-0114\(92\)90223-Q](https://doi.org/10.1016/0165-0114(92)90223-Q).
- Liu, Z., Liu, Y., 2019. A Bayesian network based method for reliability analysis of subsea blowout preventer control system. J. Loss Prev. Process. Ind. 59, 44–53. <https://doi.org/10.1016/j.jlp.2019.03.004>.
- Liu, P., Liu, Y., Cai, B., Wu, X., Wang, K., Wei, X., Xin, C., 2020. A dynamic Bayesian network based methodology for fault diagnosis of subsea Christmas tree. Appl. Ocean Res. 94, 101990. <https://doi.org/10.1016/j.apor.2019.101990>.
- Liu, J., 2021. Explainable fault diagnosis of gas-liquid separator based on fully convolutional neural network. Computers and Chemical Engineering (15).
- Liu, X., Ji, X., Lei, L., 2024. Surrogate-based drag optimization of autonomous remotely vehicle using an improved sequentially constrained Monte Carlo method. Ocean. Eng. 297, 117047. <https://doi.org/10.1016/j.oceaneng.2024.117047>.
- Abadi, M., Agarwal, A., Barham, P., Brevdo, E., Chen, Z., Citro, C., Corrado, G.S., Davis, A., Dean, J., Devin, M., Ghemawat, S., Goodfellow, I., Harp, A., Irving, G., Isard, M., Jia, Y., Jozefowicz, R., Kaiser, L., Kudlur, M., Levenberg, J., Mane, D., Monga, R., Moore, S., Murray, D., Olah, C., Schuster, M., Shlens, J., Steiner, B., Sutskever, I., Talwar, K., Tucker, P., Vanhoucke, V., Vasudevan, V., Viegas, F., Vinyals, O., Warden, P., Wattenberg, M., Wicke, M., Yu, Y., Zheng, X., n.d. TensorFlow: Large-Scale Machine Learning on Heterogeneous Distributed Systems.
- Liu, Z., Yang, X., Wu, M., Mu, W., Liu, G., 2023. Leveraging deep learning techniques for ship pipeline valve leak monitoring. Ocean Engineering 288, 116167. <https://doi.org/10.1016/j.oceaneng.2023.116167>.
- Lou, S., Yang, C., Wu, P., Kong, L., Xu, Y., 2022. Fault Diagnosis of Blast Furnace Iron-Making Process With a Novel Deep Stationary Kernel Learning Support Vector Machine Approach. IEEE Transactions on Instrumentation and Measurement 71, 1–13. <https://doi.org/10.1109/TIM.2022.3200113>.
- Meng, H., An, X., Xing, J., 2022. A data-driven Bayesian network model integrating physical knowledge for prioritization of risk influencing factors. Process Saf. Environ. Protect. 160, 434–449. <https://doi.org/10.1016/j.psep.2022.02.010>.
- Metz, L., Poole, B., Pfau, D., Sohl-Dickstein, J., Unrolled Generative Adversarial Networks. <https://doi.org/10.48550/arXiv.1611.02163>.
- Migacz, S., Dutka, K., Gumienny, P., Marchwiany, M., Gront, D., Rudnicki, W.R., 2019. Parallel implementation of a sequential Markov chain in Monte Carlo simulations of physical systems with pairwise interactions. J. Chem. Theor. Comput. 15, 2797–2806. <https://doi.org/10.1021/acs.jctc.8b01168>.
- Natarajan, S., Srinivasan, R., 2010. Multi-model based process condition monitoring of offshore oil and gas production process. Chem. Eng. Res. Des. 88, 572–591. <https://doi.org/10.1016/j.cherd.2009.10.013>.
- O'Keeffe, C.J., Orkoulas, G., 2009. Parallel canonical Monte Carlo simulations through sequential updating of particles. J. Chem. Phys. 130, 134109. <https://doi.org/10.1063/1.3097528>.
- Peng, D.-Y., Robinson, D.B., 1976. A new two-constant equation of state. Ind. Eng. Chem. Fund. 15, 59–64. <https://doi.org/10.1021/i160057a011>.
- Ren, L., Lv, W., Jiang, S., Xiao, Y., 2016. Fault Diagnosis Using a Joint Model Based on Sparse Representation and SVM. IEEE Transactions on Instrumentation and Measurement 65, 2313–2320. <https://doi.org/10.1109/TIM.2016.2575318>.
- Sahu, A.R., Palei, S.K., 2022. Fault analysis of dragline subsystem using Bayesian network model. Reliab. Eng. Syst. Saf. 225, 108579. <https://doi.org/10.1016/j.ress.2022.108579>.
- Sankarakrishnan, A., Billinton, R., 1995. Sequential Monte Carlo simulation for composite power system reliability analysis with time varying loads. IEEE Trans. Power Syst. 10, 1540–1545. <https://doi.org/10.1109/59.466491>.
- Sevee, J.E., 2010. Effective porosity measurement of a marine clay. J. Environ. Eng. 136, 674–681. [https://doi.org/10.1061/\(ASCE\)EE.1943-7870.0000205](https://doi.org/10.1061/(ASCE)EE.1943-7870.0000205).
- Shan, X., Yu, W., Gong, J., Huang, W., Wen, K., Wang, H., Ren, S., Wang, D., Shi, Y., Liu, C., 2023. A methodology to evaluate gas supply reliability of natural gas pipeline network considering the effects of natural gas resources. Reliab. Eng. Syst. Saf. 238, 109431. <https://doi.org/10.1016/j.ress.2023.109431>.
- Shao, H., Cheng, J., Jiang, H., Yang, Y., Wu, Z., 2020. Enhanced deep gated recurrent unit and complex wavelet packet energy moment entropy for early fault prognosis of bearing. Knowl. Base Syst. 188, 105022. <https://doi.org/10.1016/j.knosys.2019.105022>.
- Song, S., Liu, X., Li, C., Li, Z., Zhang, S., Wu, W., Shi, B., Kang, Q., Wu, H., Gong, J., 2023. Dynamic simulator for three-phase gravity separators in oil production facilities. ACS Omega 8, 6078–6089. <https://doi.org/10.1021/acsomega.2c08267>.
- System Reliability Theory | Wiley Series in Probability and Statistics [WWW Document], n.d. URL <https://onlinelibrary.wiley.com/doi/book/10.1002/9781119373940> (accessed 11.13.23).
- Talreja, R., 2016. Physical modelling of failure in composites. Phil. Trans. R. Soc. A. 374, 20150280. <https://doi.org/10.1098/rsta.2015.0280>.
- Tan, Y., Zhang, J., Tian, H., Jiang, D., Guo, L., Wang, G., Lin, Y., 2021. Multi-label classification for simultaneous fault diagnosis of marine machinery: A comparative study. Ocean Engineering 239, 109723. <https://doi.org/10.1016/j.oceaneng.2021.109723>.
- Tang, H.-H., Zhang, K., Wang, B., Zu, X., Li, Y.-Y., Feng, W.-W., Jiang, X., Chen, P., Li, Q.-A., 2024. Early bearing fault diagnosis for imbalanced data in offshore wind turbine using improved deep learning based on scaled minimum unscented kalman filter. Ocean. Eng. 300, 117392. <https://doi.org/10.1016/j.oceaneng.2024.117392>.
- Vaddi, P.K., Pietrykowski, M.C., Kar, D., Diao, X., Zhao, Y., Mabry, T., Ray, I., Smidts, C., 2020. Dynamic bayesian networks based abnormal event classifier for nuclear power plants in case of cyber security threats. Prog. Nucl. Energy 128, 103479. <https://doi.org/10.1016/j.pnucene.2020.103479>.
- Wang, J., Du, G., Zhu, Z., Shen, C., He, Q., 2020. Fault diagnosis of rotating machines based on the EMD manifold. Mechani. Syst. Signal Process. 135, 106443. <https://doi.org/10.1016/j.jmss.2019.106443>.
- Wang, W., He, X., Li, Y., Shuai, J., 2022. Risk analysis on corrosion of submarine oil and gas pipelines based on hybrid Bayesian network. Ocean. Eng. 260, 111957. <https://doi.org/10.1016/j.oceaneng.2022.111957>.
- Wangdee, W., Billinton, R., 2006. Bulk electric system well-being analysis using sequential Monte Carlo simulation. IEEE Trans. Power Syst. 21, 188–193. <https://doi.org/10.1109/TPWRS.2005.862000>.
- Weber, P., Medina-Oliva, G., Simon, C., Iung, B., 2012. Overview on Bayesian networks applications for dependability, risk analysis and maintenance areas. Engineering Applications of Artificial Intelligence, Special Section: Dependable System Modelling and Analysis 25, 671–682. <https://doi.org/10.1016/j.engappai.2010.06.002>.
- Wu, P., 2017. SEQUENTIAL MONTE CARLO BASED DATA ASSIMILATION FRAMEWORK AND TOOLKIT FOR DYNAMIC SYSTEM SIMULATIONS.
- Wu, Z., Li, S., 2019. Reliability evaluation and sensitivity analysis to AC/UHVDC systems based on sequential Monte Carlo simulation. IEEE Trans. Power Syst. 34, 3156–3167. <https://doi.org/10.1109/TPWRS.2019.2896228>.
- Wu, J., Shang, L., Pan, Z., Zhou, L., 2022. Energy, exergy, economic, exergoeconomic, and exergoenvironmental (SE) analyses and optimization of a novel three-stage cascade system based on liquefied natural gas cold energy. Energ. Tech. 10, 220228. <https://doi.org/10.1002/ente.202200228>.
- Xiao, Q., Li, Y., Luo, F., Liu, H., 2023. Analysis and assessment of risks to public safety from unmanned aerial vehicles using fault tree analysis and Bayesian network. Technol. Soc. 73, 102229. <https://doi.org/10.1016/j.techsoc.2023.102229>.

- Yu, W., Song, S., Li, Y., Min, Y., Huang, W., Wen, K., Gong, J., 2018a. Gas supply reliability assessment of natural gas transmission pipeline systems. *Energy* 162, 853–870. <https://doi.org/10.1016/j.energy.2018.08.039>.
- Yu, W., Wen, K., Min, Y., He, L., Huang, W., Gong, J., 2018b. A methodology to quantify the gas supply capacity of natural gas transmission pipeline system using reliability theory. *Reliab. Eng. Syst. Saf.* 175, 128–141. <https://doi.org/10.1016/j.ress.2018.03.007>.
- Yang, Z., Zhang, J., Zhao, Z., Zhai, Z., Chen, X., 2020. Interpreting network knowledge with attention mechanism for bearing fault diagnosis. *Appl. Soft Comput.* 97, 106829. <https://doi.org/10.1016/j.asoc.2020.106829>.
- Yu, W., Gong, J., Huang, W., Liu, H., Dang, F., Luo, J., Sun, Y., 2021a. A systematic methodology to assess hydraulic reliability and gas supply reliability of the natural gas pipeline network. *J. Pressure Vessel Technol.* 143, 041804 <https://doi.org/10.1115/1.4049711>.
- Yu, W., Huang, W., Wen, Y., Li, Y., Liu, H., Wen, K., Gong, J., Lu, Y., 2021b. An integrated gas supply reliability evaluation method of the large-scale and complex natural gas pipeline network based on demand-side analysis. *Reliab. Eng. Syst. Saf.* 212, 107651 <https://doi.org/10.1016/j.ress.2021.107651>.
- Zagorecki, A., Drudzsel, M.J., 2013. Knowledge engineering for bayesian networks: how common are noisy-MAX distributions in practice? *IEEE Trans. Syst. Man Cybern. Syst.* 43, 186–195. <https://doi.org/10.1109/TSMCA.2012.2189880>.
- Zhang, R., Hong, T., 2017. Modeling of HVAC operational faults in building performance simulation. *Appl. Energy* 202, 178–188. <https://doi.org/10.1016/j.apenergy.2017.05.153>.
- Zhao, Y., Wang, S., Xiao, F., Ma, Z., 2013a. A simplified physical model-based fault detection and diagnosis strategy and its customized tool for centrifugal chillers. *Faculty of Engineering and Information Sciences - Papers: Partisans A*, 283–294.
- Zhao, Y., Xiao, F., Wang, S., 2013b. An intelligent chiller fault detection and diagnosis methodology using Bayesian belief network. *Energy Build.* 57, 278–288. <https://doi.org/10.1016/j.enbuild.2012.11.007>.
- Zhou, X., Liu, H., Chen, L., Feng, D., Mou, P., 2022. Study on quantitative evaluation method for failure possibility of oil and gas gathering. *Journal of Safety Science and Technology* 18 (6), 167–171. <https://doi.org/10.11731/j.issn.1673-193x.2022.06.025>.
- Zio, E., 2013. The Monte Carlo simulation method for system reliability and risk analysis. *Springer Series in Reliability Engineering*. Springer, London. <https://doi.org/10.1007/978-1-4471-4588-2>.
- Odena, A., Olah, C., Shlens, J., 2017. Conditional Image Synthesis With Auxiliary Classifier GANs.